Comparing time-lapse crosshole GPR data collected under natural and forced infiltration conditions to estimate unsaturated soil hydraulic properties

M. Scholer[1], J. Irving[1*], M. C. Looms[2], L. Nielsen[2] and K. Holliger[1]

[1] Institute of Geophysics, University of Lausanne,

CH-1015 Lausanne, Switzerland

[2] Department of Geography and Geology, University of Copenhagen,

DK-1350 Copenhagen, Denmark

*Corresponding author: james.irving@unil.ch

July 17, 2012

Abstract

Time-lapse geophysical data acquired during dynamic hydrological experiments are being increasingly employed to estimate subsurface hydraulic properties at the field scale. In particular, crosshole ground-penetrating radar (GPR) data, collected while water infiltrates into the subsurface either by natural or artificial means, have been demonstrated in a number of studies to contain valuable information concerning the hydraulic properties of the unsaturated zone. Previous work in this domain has considered a variety of infiltration conditions and different amounts of time-lapse GPR data. However, the particular benefits and drawbacks of these different strategies as well as the impact of a variety of key assumptions remain unclear because these results of these previous studies defy a direct comparison. Here, using a Bayesian Markov-chain-Monte-Carlo (MCMC) stochastic inversion methodology, we examine the information content of time-lapse GPR data collected under three different infiltration conditions for the estimation of vadose zone hydraulic properties. In particular, we systematically analyze synthetic and field data acquired under natural loading and two rates of forced infiltration, and we consider the value of incorporating different amounts of time-lapse GPR data into the estimation procedure. Quite importantly, our results confirm that, for all infiltration scenarios considered, the time-lapse GPR data contain important information about subsurface hydraulic properties as a function of depth. However, forced infiltration is found to offer the greatest parameter refinement in both the synthetic and field examples. Considering greater amounts of time-lapse data in the inversion procedure is also found to help significantly refine the estimation of key hydraulic parameters. However, inconsistencies observed with regard to the field data point to the possibility that our inversions may be subject to structural model errors, which in turn underlines the fundamental importance of a systematic analysis of such errors for future related studies.

1. Introduction

Detailed knowledge of soil hydraulic properties, namely how the water retention and unsaturated hydraulic conductivity vary as a function of matric head, is essential for the accurate modeling of flow and transport processes in the vadose zone. Such modeling is critical for a wide variety of activities, including irrigation and fertilization management, assessment of contaminant fate, estimation of groundwater recharge for water balance calculations, and evaluation of the hydrological and agricultural impacts of climate change. To determine vadose zone hydraulic properties, a broad array of measurement techniques exist [11]. Laboratory analyses conducted on soil cores, traditionally based on hydrostatic equilibrium or steady-state flux conditions but increasingly involving transient experiments, have the advantage of being well understood, cost effective, and relatively simple to implement [e.g., 10, 51]. However, they can lead to hydraulic property estimates that are not representative of field conditions because of the associated disturbance of the soil structure [e.g., 11]. Consequently, field techniques for measuring hydraulic properties *in situ* have become popular [49]. Such methods generally involve some kind of infiltration or drainage experiment combined with dynamic tensiometer and/or time-domain reflectometry (TDR) measurements in order to determine the water retention and/or unsaturated hydraulic conductivity functions under comparatively natural conditions.

With regard to the determination of soil hydraulic properties from either laboratory or field measurements, one particular approach that has gained widespread acceptance over the past two decades is the use of inverse modeling [53]. In contrast to direct measurement techniques that generally require well controlled and rather simplistic boundary conditions and/or system states in order to implement analytical solutions, inverse modeling employs a numerical model for the hydrological experiment in order to find a set of parameters characterizing hydraulic properties that allow the best predictions of state variable

measurements. As such, it has the important advantage of accommodating more flexible and natural experimental conditions than direct measurement methods, with the trade-off of generally requiring highly accurate sensor data in time and space as input [11]. Initial work on the inverse estimation of soil hydraulic properties involved local gradient-based search algorithms [e.g., 43, 44, 55]. To better address the non-linear and non-unique nature of the inverse problems, subsequent research has focused on global optimization techniques [e.g., 1, 22, 32, 52], and most recently on stochastic inverse methods that allow for the assessment of uncertainty as well as the incorporation of prior information into the estimation procedure [e.g., 26, 38, 47, 58]. In this regard, both the pseudo-Bayesian Generalized Likelihood Uncertainty Estimation (GLUE) technique [4], as well as formal Bayesian posterior sampling using Markov-chain-Monte-Carlo (MCMC) algorithms [e.g., 29], have been considered.

A critical drawback associated with traditional hydrological methods for determining unsaturated hydraulic properties, whether these methods be laboratory or field-based and whether they employ a direct or inverse estimation approach, is the limited spatial extent of the corresponding measurements. That is, traditional hydrological methods involve either the analysis of core samples or state variable data from tensiometers and/or TDR, all of which represent a local "point" scale that may not be representative of larger-scale properties relevant to modeling interests. Indeed, small-scale heterogeneity in soil conditions can introduce large variations in the values measured using these techniques, and hence significant errors in larger-scale property estimates can arise if one of such point measurements is used to characterize a region [31]. To address this issue, a number of studies have considered averaging the results of multiple traditional hydrological measurements distributed over some spatial domain of interest [34, 38, 58]. However, such an approach is time consuming and expensive, and still runs the risk that the thus obtained properties are not representative of the larger volume. Another means of addressing this issue, which has been

the subject of much attention in recent years, is the use of geophysical methods. Geophysical survey techniques allow for the robust estimation of field-scale geophysical properties, such as the electrical conductivity or dielectric permittivity. Although not the hydraulic properties we seek, these properties are often highly correlated with soil water content, which means that they can be used to monitor changes in field-scale water content *in situ* during infiltration or drainage, and estimate hydraulic properties through an inverse modeling approach [e.g., 5, 6, 19, 20, 23, 24, 35, 56]. In this regard, the stochastic inversion of crosshole ground-penetrating radar (GPR) traveltime data is one technique that has shown much recent promise. Work in this area began with the GLUE inversion methodology for estimating the van Genuchten – Mualem (VGM) [30, 50] parameters versus depth in simple layered soils, and involved both natural loading [6, 7] and forced infiltration [24] experiments. More recently, Scholer et al. [39, 40] considered the same data sets as previous researchers, but within a formal Bayesian MCMC inversion framework, and found that a considerably greater reduction in uncertainty in VGM parameter estimates could be obtained. This was especially the case when informed, but realistic, prior information based on soil property databases was considered.

With regard to the stochastic inversion of crosshole GPR data for the estimation of subsurface hydraulic properties, there exist a number of practical issues that are critically important to address in order to obtain robust parameter estimates and further advance the methodology, but have yet to be thoroughly investigated in the existing literature. One of these issues concerns the nature of the considered hydrological experiment. As mentioned above, both natural loading and forced infiltration have been monitored with crosshole GPR methods, specifically through the collection of time-lapse zero-offset-profile (ZOP) traveltime data, for the purpose of estimating subsurface VGM parameters in layered media. However, it remains unclear what method may provide better results, and under what circumstances this will occur, because previous work has not offered the possibility of comparison. Advantages

of considering rainfall-based infiltration over forced infiltration are that the natural conditions of the system are respected, and also that flow can be better approximated as 1D because infiltration occurs over a greater spatial domain and is of generally lesser magnitude. For the sake of computational tractability, all previous work utilizing stochastic inverse methods for determining soil hydraulic properties has considered purely vertical flow models based on Richards' equation in 1D, which can represent a significant source of model structural error in cases where lateral flow is significant [e.g., 40]. On the other hand, defining the upper boundary of a natural loading experiment is more challenging than for forced infiltration because robust estimates of evapotranspiration are required. Further, smaller variations in soil water content under natural loading may result in less sensitivity to subsurface hydraulic properties, and natural loading experiments also require much longer measurement periods.

Another key question with regard to the stochastic estimation of unsaturated hydraulic properties from time-lapse crosshole GPR data, that has not been properly addressed in previous research, concerns the length of the measurement period and the incremental value of additional geophysical data. Clearly, monitoring changes in subsurface water content as infiltration occurs can provide important information on subsurface hydraulic properties, as these properties are what control the dynamic evolution of the soil water content field. However, the information content of GPR profiles collected as a function of time, with respect to how much they help to further refine hydraulic property estimates, has not been adequately assessed. For example, in the case where significant structural model errors are present, either because of inaccurate boundary condition assumptions or problems with the underlying model physics, a critical question is whether the incorporation of additional time-lapse data into the stochastic inversion procedure actually worsens at some point the obtained parameter estimates because data residuals will grow as the simulation time increases.

In this study, we begin investigation into the two important issues described above through a combined synthetic and field data analysis that takes advantage of a unique and rich set of measurements collected at the Arrenaes field site in Denmark. Time-lapse ZOP crosshole GPR traveltime data acquired during a forced infiltration experiment at this site were already considered by Looms et al. [24] and Scholer et al. [40] for the stochastic estimation of subsurface VGM parameters in a series of five subsurface layers. Here, we consider the same data plus additional GPR measurements acquired over the course of two other infiltration experiments, one involving a lesser forced infiltration rate and the other conducted under natural loading conditions. We thus have at our disposal three time-lapse ZOP crosshole GPR data sets, acquired in exactly the same location and corresponding to three different infiltration scenarios, that we use in this study to estimate subsurface VGM parameters through a Bayesian MCMC stochastic inversion approach. In addition, we consider the inversion of synthetic GPR data modeled after each of these field scenarios, for which the "true" model parameters and underlying physics and boundary conditions are completely known. We begin with an analysis of the synthetic data, which permits us to examine the results that can be obtained in the ideal case where no structural model errors are present. Next we perform the same analysis on the Arrenaes field measurements. Throughout the paper, the different results obtained are compared and contrasted in order to learn how field experiments and stochastic inversions may be best carried out for the reliable estimation of unsaturated hydraulic properties and their corresponding uncertainties.

2. Methodology

2.1 Governing equations

Estimating subsurface unsaturated hydraulic parameters from a set of depth and time-dependent crosshole GPR traveltime measurements requires establishing a link between these

parameters and the GPR data. Scholer et al. [40] describe in detail how models for the relevant hydrological and geophysical processes can be coupled through the state variable water content in order to provide such a link. Here, we summarize briefly this procedure and refer the reader to their paper for full information. Assuming that water movement in the vadose zone can be adequately described as vertical, we have as our governing hydrological process model the following 1D form of Richards' equation [33]:

$$\frac{\partial}{\partial z}\left[K(h)\frac{\partial h}{\partial z} + K(h) \right] = \frac{\partial \theta(h)}{\partial t}, \tag{1}$$

where K is the unsaturated hydraulic conductivity [LT^{-1}], h is the matric head [L], θ is the water content [L^{3}L^{-3}], z is depth [L], and t is time [T]. Note that the assumption of purely vertical flow is pervasive throughout the literature on the inverse estimation of unsaturated hydraulic parameters from geophysical and hydrological measurements [e.g., 6, 7, 24, 26, 27, 38, 58]. In the case of natural loading conditions, such an assumption is generally well justified as the precipitation covers a large area. Under forced infiltration conditions where the spatial extent of the infiltration domain is limited, however, the validity of this assumption depends on the underlying subsurface properties and boundary conditions, and in many instances significant model structural errors can result from neglecting lateral contributions to flow [e.g., 40]. Although these errors can clearly be avoided by considering infiltration in three dimensions, it is important to emphasize that the use of a 3D flow model within the context of stochastic inversion is extremely computationally demanding because of the large number of forward model calculations required. As a result, for computational tractability, we follow the vast majority of previous studies and assume that 1D flow conditions prevail in our analysis. The effects of this assumption on posterior parameter estimates are discussed later when we compare the results of inverting synthetic and field GPR data under natural loading and forced infiltration conditions.

Assuming that soil hydraulic properties can be parameterized using the VGM model [30, 50], the water retention, expressed in terms of effective saturation S_e (dimensionless), is given by

$$S_e(h) = \frac{\theta(h) - \theta_r}{\theta_s - \theta_r} = \begin{cases} (1 + |\alpha h|^n)^{-m} & \text{for } h \leq 0 \\ 1 & \text{for } h > 0 \end{cases} \tag{2}$$

where θ_r and θ_s are the residual and saturated water contents, respectively [L^{3}L^{-3}], and α [L^{-1}], m, and n (both dimensionless) are empirical shape factors with $m = 1-1/n$. The unsaturated hydraulic conductivity function is then expressed as

$$K(h) = K_s S_e(h)^l \left(1 - \left(1 - S(h)^{1/m} \right)^m \right)^2, \tag{3}$$

where K_s [LT^{-1}] is the saturated hydraulic conductivity and l (dimensionless) is also a shape factor assumed here to be equal to 0.5 [30]. A total of five parameters (θ_s, θ_r, α, K_s, and n) therefore describe soil hydraulic properties with the VGM model in our work.

To solve equation (1) for the time-varying, 1D water content distribution corresponding to a given configuration of subsurface VGM parameters and specified boundary conditions, we use the software HYDRUS-1D [45], which utilizes a Galerkin finite element method based on the mass conservative iterative scheme proposed by Celia et al. [8], and is capable of accommodating an arbitrary number of subsurface layers [e.g., 24, 38, 53, 57, 58]. From these results we then determine the soil relative dielectric permittivity, ε_r (dimensionless), versus depth for the times corresponding to each GPR measurement using the empirical relationship [12]:

$$\varepsilon_r = \left(\frac{0.1841 + \theta}{0.1181} \right)^2. \tag{4}$$

Equation (4) provides a more straightfoward link between θ and ε_r than the more commonly seen relationship of Topp et al. [48], and is nearly identical to this relationship over the range

of water contents to be encountered in the vadose zone. Next, $\varepsilon_r(z,t)$ is converted to GPR velocity, $v(z,t)$ [LT^{-1}], using the following high-frequency, low-loss approximation that is valid in most environments amenable to GPR wave propagation [e.g., 3]:

$$v = \frac{c}{\sqrt{\varepsilon_r}},$$ (5)

where c [LT^{-1}] is the speed of light in free space. Finally, to determine the crosshole GPR traveltimes for a particular measurement period, we solve the eikonal equation for the corresponding velocity field:

$$|\nabla T(\mathbf{r})|^2 = s(\mathbf{r})^2,$$ (6)

where T [T] is the traveltime of first-arriving energy from the transmitter to the receiver antenna at location $\mathbf{r}$ [L] through the slowness field $s(\mathbf{r}) = 1/v(\mathbf{r})$ [TL^{-1}]. For the ZOP measurements considered in this paper, the radar antennas are considered at the same depth in two adjacent boreholes and the traveltime between them is calculated as a function of depth. Using the eikonal equation, rather than a simple conversion of velocity to traveltime based on the transmitter-receiver distance, allows us to account for bending of the radar wavefront at interfaces across which velocity changes. Even in a layered medium using the ZOP configuration, first-arriving energy will often correspond to such refracted raypaths [e.g., 35].

2.2 Stochastic inversion procedure

We use an MCMC algorithm in this paper to generate samples from the Bayesian posterior distribution of VGM model parameters conditional to (i) prior information regarding these parameters, and (ii) a set of dynamic ZOP GPR traveltime measurements that serve as a proxy for field-scale water content as a function of depth and time over the course of infiltration. The use of Bayes' theorem to combine prior information with observed data in order to refine our state of knowledge regarding a set of model parameters is a well established procedure in

both hydrology and geophysics [e.g., 36, 58] and can be generally expressed in the following manner [e.g., 29]:

$$\sigma(\mathbf{m}) = k\,\rho(\mathbf{m})\,L(\mathbf{m}), \tag{7}$$

where $\mathbf{m}$ is a vector containing the model parameters, $\rho(\mathbf{m})$ represents the joint prior distribution for those parameters, $L(\mathbf{m})$ is the likelihood function, and k is a normalization constant that ensures that the posterior distribution $\sigma(\mathbf{m})$ integrates to unity. For the inversions presented herein, we make the common assumption of independent, identically normally distributed data residuals [e.g., 17, 29, 38, 40], which means that the likelihood function takes the following form:

$$L(\mathbf{m}) = \frac{1}{\left(2\pi\sigma_r^2\right)^{N/2}} \exp\left[-\frac{(F(\mathbf{m})-\mathbf{d})^T (F(\mathbf{m})-\mathbf{d})}{2\sigma_r^2} \right] \tag{8}$$

where $\mathbf{d}$ is a vector of length N containing the observed data, σ_r^2 is the estimated residual variance, and $F(\mathbf{m})$ is the "forward model" linking a given set of model parameters to the corresponding predicted data. In our case, $F(\mathbf{m})$ represents the previously described hydrological and geophysical operators linking a particular configuration of subsurface VGM model parameters to the corresponding set of dynamic ZOP traveltime measurements.

To sample from the posterior distribution in equation (7), we use the same MCMC methodology as described by Scholer et al. [40], whereby proposed sets of VGM model parameters are accepted or rejected using a Metropolis decision rule and model perturbations are performed through a bounded symmetric proposal density function. Again, the reader is referred to their paper for full details. In short, the algorithm proceeds as follows:

1. Propose a new set of model parameters $\mathbf{m}'$, conditional on the current point in the Markov chain $\mathbf{m}$, by drawing from the proposal density $Q(\mathbf{m}'|\mathbf{m})$, which is defined to be a bounded uniform distribution centered on $\mathbf{m}$ whose width is chosen such that

the size of the model perturbations allows for a reasonable rate, typically around 30%, of accepted transitions in the MCMC procedure [13].

2. Randomly decide whether to stay at the current model $\mathbf{m}$, or to replace $\mathbf{m}$ with $\mathbf{m'}$, using the decision rule of Metropolis et al. [28] for which the transition probability is given by

$$P_{\mathbf{m}\rightarrow\mathbf{m'}} = \min\left(1, \frac{\rho(\mathbf{m'})\,L(\mathbf{m'})}{\rho(\mathbf{m})\,L(\mathbf{m})}\right). \qquad (9)$$

3. Repeat Steps 1 and 2, collecting model parameter samples in the Markov chain with each iteration, until "burn-in" has been reached and a sufficient number of posterior parameter realizations have been generated for analysis.

To determine the "burn-in" period for our inversions, that is, the point at which states in the Markov chain become independent of the starting set of model parameters and truly represent samples from the Bayesian posterior distribution, we examine the values of each model parameter versus iteration number for several parallel-running chains with random starting points and determine when the chains reach a similar equilibrium state [e.g., 14, 16]. Once the samples before burn-in have been discarded, the same number of independent posterior samples are required in our analysis to perform a valid statistical comparison of the inversion results obtained using different input data. However, the nature of the way models are proposed in the MCMC procedure means that posterior chain will exhibit a significant amount of autocorrelation. As a result, we "thin" the chain based on the maximum observed autocorrelation lag in order to obtain an approximately independent set of posterior samples.

2.3 Output analysis

Again, our aim in this study is to practically investigate the effects of different infiltration scenarios on the posterior VGM parameter estimates obtained from the stochastic inversion of

time-lapse crosshole GPR data, as well as the incremental value of these data as a function of time towards resolving the parameters. To this end, we require a means of comparing the different sets of posterior realizations obtained through the Bayesian MCMC inversion procedure. A number of possibilities exist in this regard, arguably the most intuitive of which is the straightforward comparison of marginal posterior histograms for each model parameter of interest [e.g., 21, 40]. However, the relatively large number of VGM parameters to be estimated in this study (25 for our synthetic example and 35 for the Arrenaes field case), combined with the wide range of infiltration and GPR data combinations considered (15 for the synthetic and 13 for the field) meant that this was not practical. Instead, for conciseness and greater ease of direct comparison, we follow Beven and Binley [4] and quantify the spread of the different marginal VGM posterior distributions using the Shannon entropy measure [18]. The Shannon entropy H of a discrete variable X with possible states $\{x_1, x_2, ..., x_M\}$ and corresponding probability function $p(X)$ is defined as:

$$H = -\sum_{i=1}^{M} p(x_i) \log_2 p(x_i).$$

(10)

In our case, the states x_i represent posterior marginal histogram bins where, for a particular VGM parameter, the probability of occurrence is given by

$$p(x_i) = \frac{\# \text{ of posterior realizations in the bin}}{\text{total} \# \text{ of posterior realizations}}.$$

(11)

The Shannon entropy has a maximum, $H_{max} = \log_2(M)$, when all M states are equally likely (e.g., if the posterior marginal histogram for a particular VGM parameter is uniform). Conversely, H has a minimum, $H_{min} = 0$, when one single state has a probability of one and all others have a probability of zero (e.g., when all of the posterior parameter realizations fall into a single histogram bin). The fact that H is bounded in this manner, along with the fact that its value is not dependent on the magnitude of the parameter being investigated, mean that it can be used as a convenient and comparable measure of refinement of the posterior marginal

VGM parameter distributions. It is important to note, however, that H reflects only the spread of these distributions, and says nothing regarding the accuracy of the posterior parameter estimates, which must be quantified via other means.

3. Synthetic study

3.1 Considered experiments and data

To begin our investigation into the effects of different infiltration and time-lapse scenarios on the VGM parameter estimates obtained from ZOP crosshole GPR traveltime data, we first consider a synthetic study where we have perfect knowledge of the physics and boundary conditions of the infiltration process. In this way, model structural errors are nonexistent and we begin our analysis with a best-case scenario before moving to the case of field data where such errors cannot be avoided. Table 1 shows the five-layer subsurface structure and corresponding "true" VGM parameters that were utilized for this synthetic study. For ease of comparison with the field results presented in the following section, the parameter values were chosen in accordance with sedimentological information from the Arrenaes site, and such that the simulated GPR data showed an approximately similar trend to those measured in the field. For the GPR experiment, we also consider a similar setup to that used at the Arrenaes site [25], involving boreholes 5 m apart and 12 m deep.

As mentioned previously, we consider three different infiltration cases in this paper: natural loading, which is hereby referred to as NL, and forced infiltration under two different, constant loading rates, which are hereby referred to as F1 (moderate loading) and F2 (heavy loading). Table 2 provides details on how these infiltration cases were implemented in our synthetic study, as well as the times that the corresponding GPR data were simulated. For the NL case, infiltration was considered over a one year period based on daily rainfall minus estimated evapotranspiration data obtained from the Danish Meteorological Institute (DMI)

for the Arrenaes site [37]. Figure 1 shows the daily infiltration rate for the period from 01/07/2004 to 30/07/2005, which was used to define the upper model boundary in this case. Crosshole GPR profiles were simulated at 1, 3, 6, 9, and 12 months. For the two forced infiltration cases, constant flux boundary conditions were assumed along the upper model surface with infiltration rates for F1 and F2 of 0.1 cm/h and 0.4 cm/h, respectively. Here, a 20-day experiment was considered, and GPR profiles were generated daily. The forced infiltration was stopped after 10 days in order to simulate drainage conditions over the last half of the experiment.

To generate the synthetic time-lapse ZOP crosshole GPR traveltime data corresponding to each infiltration case described in Table 2, we first used HYDRUS-1D with a vertical cell discretization of 0.03 m in order to obtain the time-varying distribution of water content in the subsurface over the considered simulation period. The time step was calculated adaptively by the software and constrained by a series of output times of interest. Note that a 1D flow model was utilized for the generation of the synthetic data in order to be consistent with the purely vertical flow assumption in our MCMC analysis and thus avoid, for this synthetic study, model errors related to the 1D approximation. For all three infiltration cases considered, the lower model boundary was set at 16 m depth and specified to have a free drainage condition. The initial conditions were defined to be the water content profile obtained after a pre-infiltration period of one year using net infiltration estimates at the Arrenaes site from 01/07/2003 to 01/07/2004 [37]. Next, to convert the resulting time-varying water content profiles to radar velocity at the times corresponding to the collection of crosshole GPR data, we used equations (4-6). For the subsequent simulation of ZOP GPR traveltimes with the PRONTO eikonal solver [2], the grid discretization was set to 0.1 m and the transmitter and receiver antennas were assumed to be moved at 0.25 m increments along the left- and right-hand model edges from to 1.5 to 12 m depth. This yielded 43 ZOP

traveltime measurements per profile. Finally, Gaussian random noise with a standard deviation equal to 1% of the mean overall traveltime value was added to the resulting data to simulate more realistic conditions.

Figure 2 shows the simulated ZOP crosshole GPR traveltime data as a function of depth and time corresponding to the three different infiltration cases. Again, these data are strongly related to soil water content, with greater traveltimes indicating wetter materials. For the NL case, little variation in the data is observed over time because of the relatively small infiltration rates considered (Figure 1). As a result, we do not anticipate in this case that the consideration of additional GPR profiles with time in the inversion procedure should provide much additional independent information regarding the hydraulic characteristics of the various soils (e.g., [6]). For the F1 case, on the other hand, the GPR traveltime data can be seen to exhibit significant temporal variation as the water front moves through the system. We thus expect in this case that the consideration of greater amounts of time-lapse data should help to noticeably refine the VGM parameter estimates in the different layers. The traveltime data for the F2 case show the greatest temporal variation because of the large infiltration rate and corresponding stressing of the system, and intuitively should offer the highest potential for VGM parameter refinement. Notice in Figure 2 that, for the F1 and F2 cases, desaturation is seen after 10 days because the infiltration was stopped. Also notice that, for all three infiltration cases, the five subsurface layers can be easily identified because of the different hydraulic behavior of the soils and the corresponding differences in their water contents versus depth. Although not important for our synthetic study, this latter fact plays a key role when defining the hydraulically significant subsurface layering in the field for the inversion of the Arrenaes field data in Section 4.

3.2 Bayesian MCMC inversion

The previously described Bayesian MCMC inversion strategy was used to estimate the VGM parameters in each subsurface layer from the three ZOP crosshole GPR data sets shown in Figure 2. As mentioned, in addition to examining the effects of different infiltration rates on the posterior parameter estimates, we wish to assess the incremental value of the time-lapse GPR data on our ability to resolve the parameters. To this end, five different inversion scenarios for the NL, F1, and F2 cases were considered, each involving a different amount of time-lapse data as input into the MCMC procedure. Table 3 summarizes the resulting 15 different inversions that were performed in our synthetic study. For each of the five time-lapse scenarios, the table indicates the time up to which GPR data were considered, as well as the corresponding number of ZOP profiles. The same number of profiles were used in every scenario to be able to effectively compare results across the three different infiltration cases.

For all 15 stochastic inversions, the same uniform prior distribution for the VGM parameters in each layer was assumed. This prior, which represents a relatively broad range of values and encompasses a wide variety of soil types (e.g., sand, silt, clay), is in good agreement with the non-informative priors used in previous work in this domain [e.g., 7, 24, 38]. Although Scholer et al. [39, 40] found that significantly improved VGM parameter estimates could be obtained from crosshole GPR traveltime data through the consideration of informed correlated prior distributions based on soil property databases, we chose here to work with a uniform prior in order to better assess the information content of the GPR data alone [40]. Table 4 shows the lower and upper limits of our assumed prior distribution. Because the upper boundary of θ_r must be smaller than the initial water content, we defined it as follows: 0.08 for Layer 1, 0.06 for Layer 2, 0.08 for Layer 3, 0.13 for Layer 4 and 0.08 for Layer 5.

In the Bayesian MCMC inversion procedure, we assumed to have exact knowledge of the 5-layer subsurface structure and corresponding boundaries given in Table 1. The residual

standard deviation, σ_r, in equation (8) was defined based on the errors prescribed to the GPR traveltime measurements, and was thus set equal to 1% of the overall mean traveltime value. For each inversion described in Table 3, six different Markov chains were initiated with different random starting points in order to determine when burn-in had been achieved and to speed the subsequent generation of posterior model parameter samples. After burn-in, 100,000 iterations were then run for each chain. Based on the autocorrelation analysis of the results, we considered every 1000 samples to thin the chains, which resulted in a total number of 600 approximately independent posterior samples for analysis per inversion.

3.3 Results

Figure 3 shows the Shannon entropy measures that were calculated for the VGM parameters in each of the 5 layers from the results of the 15 different stochastic inversions. To obtain these values, the posterior samples for each parameter were binned into 120 equal intervals between the minimum and maximum considered values (Table 4), and H was calculated using equations (10) and (11). The maximum possible value for the Shannon entropy in our synthetic study, which corresponds to the uniform prior distribution and is shown as Scenario 0, is $H_{max} = \log_2(120) = 6.9$. The decrease in H from this value for the different considered cases is a measure of the refinement, or reduction in spread, of the VGM parameter distributions through the incorporation of the GPR data. Again, however, H says nothing regarding the accuracy of the posterior parameter estimates. This important component of our analysis will be considered in Figures 4 through 6.

Notice in Figure 3 that, for each infiltration case and time-lapse scenario considered, the value of H is always lower than H_{max}, which means that incorporation of the GPR data into the inversion procedure consistently allows for some reduction of uncertainty regarding the VGM parameters past the assumed prior distribution. Even for Scenario 1 where only one

GPR profile, simulated shortly after the start of infiltration, was used as input into the Bayesian MCMC algorithm, we observe a slight to moderate decrease in H from its maximum value for all VGM parameters. This is despite the fact that, for the forced infiltration cases, the water front had not yet passed through Layers 3, 4, and 5 after only one day. Indeed, differences between predicted and observed GPR traveltimes in the inversion procedure, even at early times in layers below the infiltrating water front, can provide important information regarding the VGM parameters in these layers [39, 40]. For example, a predicted change from the initial traveltime distribution after just one day in Layer 4, which is not seen in the observed traveltime data for Day 1, would indicate that the proposed set of VGM parameters in that layer is unlikely and should probably be rejected.

Also notice in Figure 3 that, as additional time-lapse GPR data are considered past Scenario 1 for each infiltration case, the VGM parameter distributions become further refined, as indicated by the general decrease in H with increasing scenario number. This could be expected, as the consideration of a greater number of consistent data in the inversion procedure should allow for further reduction in posterior uncertainty. However, it is important to note that the data from some time periods and infiltration cases appear to bring more than the data from others. For example, in moving from Scenario 4 to Scenario 5 for the F2 case, which corresponds to adding GPR data collected under drainage conditions after a high rate of forced infiltration, we significantly reduce the calculated value of H for almost all of the VGM parameters, generally more than when we move between other scenarios (e.g., Scenario 3 to Scenario 4). This suggests that the monitoring of drainage at the field scale using GPR, in addition to infiltration, may offer valuable additional information regarding subsurface hydraulic properties [e.g., 9, 46], which to our knowledge has not yet been considered in the context of a geophysical field study. We also observe that, generally speaking, the monitoring of forced infiltration over only 10 days appears to allow for more VGM parameter refinement

than the monitoring of natural loading over 9 months, as the *H* values in Scenario 4 corresponding to the NL case tend to be higher on average than those calculated for F1 and F2. This likely results from the greater temporal changes in subsurface water content in the forced infiltration cases (in particular F2), which have the effect of increasing the sensitivity of the GPR traveltime data to small changes in the VGM parameters. Indeed, in almost every instance in Figure 3, the *H* values calculated for Scenario 5 for the F2 case are also lower than those corresponding to F1.

In order to quantify not only the spread of the posterior VGM parameter distributions obtained from the 15 different stochastic inversions, but also the accuracy of these distributions, Figure 4 shows the posterior means and standard deviations that were obtained for the parameters in Layer 3, along with the corresponding true values from Table 1. Only the results for Layer 3 are shown for the sake of conciseness; however, similar conclusions can be drawn for the other layers. As was observed in Figure 3, we see that considering just Scenario 1 already provides us with important information about the VGM parameters in each layer past the uniform prior distribution. As additional time-lapse GPR data are incorporated into the inversion procedure, the uncertainties around the mean values then tend to become increasingly reduced. Again, this could be expected because subsequent scenarios represent greater amounts of input data. However, note that (i) the uncertainty is reduced markedly less with scenario number for the NL case than for the F1 and F2 cases, and (ii) the F2 case tends to offer the best parameter refinement. We also see in Figure 4 that, quite importantly, all of the VGM parameters in Layer 3 appear to be properly estimated through the Bayesian MCMC inversion procedure, in the sense that the posterior means generally match the true parameter values, especially as the scenario number increases. Indeed, as greater amounts of time-lapse data are considered in the inversion, especially for the F1 and F2 cases, the posterior means

can be generally seen to gradually and consistently approach the correct values, which clearly indicates the value of the additional data towards resolving the soil hydraulic properties.

Finally, Figures 5 and 6 offer arguably the best means of quantifying how much information the different sets of time-lapse ZOP GPR data bring to characterize vadose zone hydraulic behavior, as they show the water retention and unsaturated hydraulic conductivity functions corresponding to the posterior VGM parameter samples obtained in each of the 15 different inversions, along with the range of possibilities for these functions that is consistent with the prior distribution in Table 4. Again, for the sake of conciseness, only Layer 3 is considered, but similar conclusions can be drawn for the other layers. Consistent with what was observed in Figures 3 and 4, we see in Figures 5 and 6 that the soil hydraulic properties become increasingly refined from the uniform prior as more time-lapse GPR data are included into the inversion procedure, with higher infiltration rates generally offering greater curve refinement as the scenario number increases. The water retention and unsaturated hydraulic conductivity curves also tend to be correctly estimated, as indicated by the fact that the true curves consistently lie near the center of the 95% posterior uncertainty bounds, even when these bounds have been noticeably reduced.

To summarize, the results of our synthetic study have shown that time-lapse GPR data, collected over the course of infiltration, can offer valuable information regarding field-scale unsaturated hydraulic properties versus depth, and that the information content of these data is significantly increased when relatively high rates of forced infiltration are monitored over a short time period, as opposed to the long-term monitoring of natural loading. Note, however, that these findings correspond to an ideal case where model structural errors have been purposely avoided in the inversion procedure to assesss the maximum potential of the GPR measurements. Next, we proceed to examine the validity of these results in the context of field

GPR measurements acquired at the Arrenaes site in Denmark, with the overreaching aim of identifying important directions for future work in this domain.

4. Application to field data

4.1 Field site and data

The Arrenaes field site was developed to study flow and transport processes in the unsaturated zone using a variety of geophysical and hydrological measurement techniques, and has been the subject of a number of previous studies [24, 25, 40]. Figures 7a and 7b show the overall location of this site in Denmark and the eight boreholes that have been installed there, respectively. Along each line of the cross in Figure 7b, the outer two boreholes (7 m apart) were equipped for crosshole ERT measurements whereas the two inner boreholes (5 m apart) were intended for crosshole GPR measurements. Borehole A was cored for sedimentological analysis. Figure 8 shows the grain size statistics and material percentages that were determined every 30 cm down Borehole A [15]. The subsurface at the site is mainly characterized by layered alluvial sand sediments with minor fractions of silt and clay (see table 5). Year-round, the water table is located at approximately 30 m depth.

From July 2004 to November 2005, three time-lapse crosshole GPR data sets were acquired at the Arreneas site over the course of three different infiltration experiments, with the overall goal of using these data to estimate subsurface unsaturated hydraulic properties at the field scale. One of these experiments involved natural loading (NL), whereas the other two were conducted under moderate (F1) and heavy (F2) forced infiltration. Table 6 provides details on these experiments, along with the timing of the GPR data acquisition. For the NL case, six GPR data sets were acquired over a one year period from July 2004 to July 2005. Again, Figure 1 shows the net daily infiltration estimates at the Arrenaes site during this time. Because previous researchers [6, 7] encountered significant difficulties in resolving

unsaturated hydraulic parameters under natural loading conditions at other field sites, and because the data in Figure 1 are subject to a significant amount of uncertainty as they depend on accurate estimates of evapotranspiration, it was decided in August 2005 to conduct a forced infiltration experiment (F1) at the site over a period of 11 days. In this case, water was infiltrated at a constant rate of 0.20 cm/h over a 7.33 x 7.33 m area using a network of drippers, and GPR data were collected daily until Day 9, after which they were collected on Day 11. Finally, in order to even further increase the water content variation in the subsurface, a second forced infiltration experiment (F2) utilizing a higher infiltration rate of 0.36 cm/h was performed at the Arrenaes site in October 2005 over a period of 20 days. The corresponding GPR data were collected daily until Day 10, after which they were collected on Days 13, 15, 17, and 20. In this study, we focus on the GPR data acquired during all three infiltration experiments between boreholes GPR1 and GPR3 (Figure 7), which were obtained using a Sensors and Software PulseEkko borehole radar system with 100 MHz antennae and a vertical antenna increment of 0.25 m between 1.5 and 12 m depth. This yielded 43 traveltime measurements per ZOP profile.

Figure 9 shows the ZOP crosshole GPR traveltime measurements as a function of depth and time corresponding to the three field infiltration experiments at the Arrenaes site. Similar to our synthetic study, not much variation is observed in the traveltime data for the NL case because of the relatively low infiltration rate (Figure 1). For the F1 and F2 cases, on the other hand, the data are again seen to exhibit significantly more variation as the water front moves through the subsurface. Note that no effects of desaturation are observed for the forced infiltration cases in our field study because infiltration was constant throughout the entire GPR measurement period. Also note that, based on each of the traveltime images in Figure 9, a number of hydraulically significant subsurface layers can be easily identified. This information, along with the grain size and sediment analysis presented in Figure 8, were used

to define a 7-layer subsurface structure that was assumed in all of our stochastic inversions (Table 5). Finally, it is important to emphasize that the GPR data obtained for the F2 case were initially presented in Looms et al. [25] and were considered within a stochastic inversion context to estimate subsurface VGM parameters by Looms et al. [24] and Scholer et al. [40]. However, the NL and F1 traveltime data in Figure 9 have never been presented, and the current work represents a unique opportunity where all three coincident data sets can be analyzed and compared within the same inversion framework.

4.2 Bayesian MCMC inversion

An important practical issue arising when considering the stochastic inversion of the Arrenaes field data collected under forced infiltration conditions, that was not encountered in our synthetic study, is the validity of the 1D flow assumption in our MCMC analysis. Because of the changes in subsurface hydraulic properties with depth and the limited lateral extent of the infiltration domain, the flow induced by the forced infiltration experiment was not purely vertical. Indeed, with regard to the F2 data set, Looms et al. [24] observed that, because of lateral spreading as a result of the presence of clay in the first 1.5 m, the water accumulation rate calculated from the GPR data over the first 5 days was smaller than the input infiltration rate of 0.36 cm/h. They also observed that, after 5 days when the infiltration front reached the finer-grained sand layer at ~8 m depth, the water front began to spread laterally. To fully account for this behavior in the inversion procedure, a 3D flow model would be required. However, as mentioned previously, it is extremely computationally demanding to consider such a model within a stochastic inversion framework. As a result, in their Bayesian MCMC analysis of the F2 data set, Scholer et al. [39] utilized a 1D numerical flow model to perform the inversions, and attempted to correct for the corresponding loss of water from lateral spreading by estimating an effective infiltration rate from the time-lapse GPR data under the

assumption of 1D flow. In tests on synthetic data, this approximation was demonstrated to allow for the reasonably accurate estimation of the VGM parameters in each subsurface layer [40]. We do the same in this paper and assume effective 1D infiltration rates of 0.10 cm/h and 0.24 cm/h for the F1 and F2 cases, respectively. For more details on how these values were calculated, please see Scholer et al. [40].

As in our synthetic study, we assess the value of additional field GPR profiles with time towards estimating the VGM parameters for each infiltration experiment. To this end, we considered five different time-lapse scenarios for the NL case, and four different scenarios for the F1 and F2 cases. Table 7 describes the resulting 13 different inversions that were performed. The same forward modeling procedure and broad uniform prior distribution as described in the synthetic example were considered for our field study. The residual standard deviation, σ_r, in equation (8) was set equal to 0.8 ns, as calculated by Looms et al. [24] based on estimates of the traveltime picking error for the GPR first arrivals. For each of the 13 inversions, six Markov chains were again initiated with different random starting points. After burn-in had been achieved, approximately 170,000 iterations were then run for each chain. Based on the autocorrelation analysis of the results, every 1000 samples were subsequently taken to thin the chains, which resulted in a total of 1000 approximately independent posterior samples per inversion.

4.3 Results

Figure 10 shows the Shannon entropy measures that were calculated for the VGM parameters in each of the 7 layers at the Arrenaes site from the results of the different stochastic inversions described in Table 7. To obtain these values, the posterior samples for each parameter were again binned into 120 equal intervals, yielding a maximum possible value for the Shannon entropy of $H_{max} = \log_2(120) = 6.9$. As seen with the synthetic data, we observe

that for each infiltration case and time-lapse scenario considered, the value of H is consistently lower than H_{max}, which indicates that incorporation of the GPR data always allows for some parameter refinement past the uniform prior distribution. We also see that, again, the VGM parameters tend to be generally further refined as greater amounts of dynamic data are added into the inversion, with some data appearing to bring more refinement than others. Note, however, that, compared with our synthetic study, the trend of the Shannon entropy with scenario number is significantly worse for the Arrenaes field data, in the sense that H can be seen in many cases to increase between adjacent scenarios as more data are considered. That is, we sometimes see a significant decrease in posterior parameter refinement as more GPR data are incorporated into the inversion procedure (e.g., from Scenario 3 to 4 for parameter n in the F1 case). We believe that this seemingly inconsistent behavior can be explained by the presence of model structural errors in our field inversions. Such errors would allow for VGM parameter refinement when using early subsets of the data that may be inconsistent with the GPR data acquired at later times. Indeed, model structural errors arising from, for example, inaccurate evapotransporation estimates in the NL case or the strictly 1D flow assumption under forced infiltration conditions, or even the chosen 7-layer model parameterization, will tend to result in residual uncertainties that grow in a complicated manner as time increases. This type of behavior was not incorporated into the relatively simple model likelihood function in equation (8) that was considered in our MCMC inversions, and in fact in the vast majority of existing literature on stochastic inversions including hydrological and geophysical data only a few studies have recently started to consider the effect of model error [e.g., 41]. Nonetheless, Figure 10 clearly indicates that, similar to the results of our synthetic study, the GPR data acquired under forced infiltration over approximately 10 days allow for substantially more VGM parameter refinement than the natural loading data acquired over many months, as the H values for Scenario 4 corresponding

to the NL case are consistently higher than those determined for F1 and F2, with F2 offering the lowest values.

Figure 11 shows the posterior VGM parameter means and standard deviations for the different time-lapse scenarios and infiltration cases described in Table 7. As in the synthetic study, we show only the results obtained for Layer 3 for the sake of conciseness, but note that similar conclusions can be made for the other layers. Notice again that, in most cases, considering just Scenario 1 provides a considerable reduction in posterior uncertainty past the uniform prior distribution. In progressing from Scenario 1 to Scenario 4, we then see a substantial decrease in the spread of the posterior distributions for the forced infiltration cases, with F2 offering the greatest parameter refinement after a 10-day period. Conversely, in the NL case, little if nothing appears to be gained in terms of parameter refinement between Scenarios 1 and 5. In fact, the posterior uncertainty is actually noticeably increased for parameter θ_r. We also see in Figure 11 that significant inconsistencies exist in the parameter estimates between the NL and forced infiltration cases; most notably, the mean value of θ_r estimated in the NL case in Scenario 4 is significantly lower than that estimated for the F1 and F2 cases. Additional inconsistencies are observed as greater amounts of time-lapse data are considered in the inversion procedure, as indicated by the strong variation in posterior mean values that often exists between adjacent scenario numbers (e.g., parameters θ_r and θ_s for the F2 case). Again, such inconsistent behavior was not observed in our synthetic study, and we feel it points to the important issue of model error that is certainly propagating as a function of time in the case of our field inversions. As a result, it is difficult to have complete confidence in the stochastic inversion results obtained for the Arrenaes data, even if a significant amount of reduction in posterior uncertainty has been obtained. For example, if posterior means vary as a function of the number of input data, what does it say about the robustness of these estimates, and how can we properly design a time-lapse experiment for accurate parameter

estimation? These findings were not evident in the work of Scholer et al. [40], and can only be assessed through the incremental analysis considered here.

Finally, Figures 12 and 13 show the water retention and unsaturated hydraulic conductivity functions for Layer 3 corresponding to the posterior VGM parameter samples obtained from each of the 13 considered inversions, along with the range of possibilities consistent with the prior distribution in Table 4. From these figures, we see that adding more data in the inversion for NL and F1 doesn't really help to further refine the soil hydraulic properties. In fact, the posterior uncertainty of the hydraulic conductivity function seen for Scenario 3 is increased compared to the one obtained for Scenario 2 in the F1 case. After Scenario 3, F2 appears to be better refined than F1 and NL. Inconsistencies can also be seen between the estimated soil hydraulic properties with time as more data are added and also between the different infiltration scenarios. For example, the posterior water retention functions obtained for Scenario 2 show a different behavior as the one obtained for Scenario 3 in the F2 case. Significant differences can also be observed between the posterior water retention functions obtained for NL, F1 and F2 for Scenario 4.

5. Discussion and conclusions

Based on targeted studies on both data, we have seen that time-lapse ZOP crosshole GPR traveltime data acquired under three different infiltration conditions universally contain valuable information regarding subsurface hydraulic properties as a function of depth. In general, higher moisture content variations in the subsurface caused by greater forced infiltration rates were seen to allow for noticeably greater reductions in posterior VGM parameter uncertainty than natural loading conditions. Moreover, the corresponding parameter estimates were found to be remarkably accurate in the case of our synthetic study. This confirms the prevailing intuition that the more pronounced changes in water content

associated with an increased stressing of a hydrologic system should allow for better resolution of the VGM parameters estimated from time-lapse GPR data [6, 7, 24]. It does, however, not give any indication as to whether the corresponding values obtained under forced infiltration are adequately representative of natural conditions. Indeed, some previous work showed that considering different infiltration conditions modified the soil hydraulic properties [54, 55]. One observed effect was that the estimated K_s increased with higher infiltration rate, which is actually similar to what we observe in our results. This is clearly a topic requiring further investigation at the field scale, and it may in fact explain some of the inconsistencies observed in the VGM parameter estimates between the different infiltration cases in our field study.

We also clearly observed in our synthetic study that incorporating more time-lapse data into the stochastic inversion procedure helped to further refine the VGM parameters, which can be attributed to two effects. First, we have the simple fact that, as more data are considered for a particular measurement configuration, the more confident we become in that measurement. Thus, the simple act of adding more of the same data into the inversion will tend to reduce posterior uncertainty. Second and more importantly, data from different time periods, especially for the forced infiltration cases, contain different, independent information regarding the unsaturated hydraulic properties. This allowed for a greater refinement of the VGM parameters for the F1 and F2 cases than for the NL case, as the denser temporal sampling allowed for capturing the water front moving downwards through the layers and gave a more complete description of the flow behavior. In fact, the consideration of drainage in our synthetic study was shown to provide a significant further reduction in spread of the posterior parameter distributions, and should be strongly considered for future field investigations.

In the case of the Arrenaes field data, the systematic reduction of posterior VGM parameter uncertainty with an increasing number of time-lapse measurements was not nearly as clear. In fact, in many instances, the spread of the posterior distributions actually increased as new data were added. Further, the posterior means were observed to change quite significantly between the various scenarios, and significant differences were seen in the parameter estimates for the different infiltration cases considered in this study. These inconsistencies can be largely explained by the assumptions that were made in order to perform our inversions, which may lead to significant model structural errors in the field study. With regard to the 1D flow assumption, we expect associated model errors to be minimal for the NL case. On the other hand, such errors are critically important for the F2 case when additional time-lapse data that are strongly affected by lateral spreading are included. In order to be able to use time-lapse ZOP GPR traveltime data collected in the field for the robust estimation of unsaturated hydraulic properties, a systematic analysis of the propagation of the model error with time and depth should be performed. A few recent studies in hydrology have started to include such error analyses when performing their stochastic inversion [e.g., 41, 42] and have also evidenced the importance of accounting for such errors.

Acknowledgments

References

[1] Abbaspour KC, Schulin R, van Genuchten MT. Estimating unsaturated soil hydraulic parameters using ant colony optimization. Adv Water Resour 2001;24:827-41.
[2] Aldridge DF, Oldenburg DW. Two-dimensional tomographic inversion with finite-difference traveltimes. J Seism Explor 1993;2:257-74.
[3] Annan AP. GPR Methods for Hydrogeological Studies. In: Rubin Y, Hubbard SS, editors. Hydrogeophysics, Dordrecht, the Netherlands: Springer; 2005, p. 185-213.
[4] Beven KJ, Binley AM. The future of distributed models - Model calibration and uncertainty prediction. Hydrol Process 1992;6:279-98.
[5] Binley AM, Cassiani G, Middleton RT, Winship P. Vadose zone flow model parameterisation using cross-borehole radar and resistivity imaging. J Hydrol 2002;267:147-59.
[6] Binley AM, Beven KJ. Vadose zone flow model uncertainty as conditioned on geophysical data. Ground Water 2003;41:119-27.
[7] Cassiani G, Binley AM. Modeling unsaturated flow in a layered formation under quasi-steady state conditions using geophysical data constraints. Adv Water Resour 2005;28:467-77.
[8] Celia MA, Bouloutas ET, Zarba RL. A General Mass-Conservative Numerical-Solution for the Unsaturated Flow Equation. Water Resour Res 1990;26:1483-96.
[9] Comegna V, Damiani P, DAnna F, Ruggiero C. Comparison of different field methods for determining the hydraulic conductivity curve of a volcanic Vesuvian soil. Geoderma 1996;73:231-44.
[10] Dane JH, Hopmans JW. Water retention and storage - Laboratory methods. In: Dane JH, Topp GC, editors. Methods of Soil Analysis, Part 4, Physical Methods, Madison, Wis.: Soil Sci Soc of Am; 2002, p. 675-720.
[11] Durner W, Lipsius K. Determining soil hydraulic properties In: Anderson MG, editor. Encyclopedia of hydrological sciences, John Wiley & Sons; 2005.
[12] Ferré PA, Rudolph DL, Kachanoski RG. Spatial averaging of water content by time domain reflectometry: Implications for twin rod probes with and without dielectric coatings. Water Resour Res 1996;32:271-9.
[13] Gilks WR, Richardson S, Spiegelhalter D. Markov Chain Monte Carlo in Practice. London: Chapman & Hall/CRC; 1996.
[14] Gilks WR, Richardson S, Spiegelhalter D. Introducing Markov chain Monte Carlo. In: Gilks WR, Richardson S, Spiegelhalter D, editors. Markov chain Monte Carlo in practice, London: Chapman&Hall/CRC; 1996, p. 1-19.
[15] Haarder EB, Binley A, Looms MC, Doetsch J, Nielsen L, Jensen KH. Comparing plume characteristics inferred from cross-borehole geophysical data. Vadose Zone J 2012;in press.
[16] Hassan AE, Bekhit HM, Chapman JB. Using Markov Chain Monte Carlo to quantify parameter uncertainty and its effect on predictions of a groundwater flow model. Environ Modell Softw 2009;24:749-63.
[17] Irving J, Singha K. Stochastic inversion of tracer test and electrical geophysical data to estimate hydraulic conductivities. Water Resour Res 2010;46:W11514.
[18] Klir GJ, Folger TA. Fuzzy sets, uncertainty and information. Englewood Cliffs: Prentice Hall; 1988.
[19] Kowalsky MB, Finsterle S, Rubin Y. Estimating flow parameter distributions using ground-penetrating radar and hydrological measurements during transient flow in the vadose zone. Adv Water Resour 2004;27:583-99.

[20] Kowalsky MB, Finsterle S, Peterson J, Hubbard S, Rubin Y, Majer E, et al. Estimation of field-scale soil hydraulic and dielectric parameters through joint inversion of GPR and hydrological data. Water Resour Res 2005;41:W11425.

[21] Laloy E, Vrugt JA. High-dimensional posterior exploration of hydrologic models using multiple-try DREAM(ZS) and high-performance computing. Water Resour Res 2012;48:W01526.

[22] Lambot S, Javaux M, Hupet F, Vanclooster M. A global multilevel coordinate search procedure for estimating the unsaturated soil hydraulic properties. Water Resour Res 2002;38:1224.

[23] Lambot S, Antoine M, van den Bosch I, Slob EC, Vanclooster M. Electromagnetic inversion of GPR signals and subsequent hydrodynamic inversion to estimate effective vadose zone hydraulic properties. Vadose Zone J 2004;3:1072-81.

[24] Looms MC, Binley AM, Jensen KH, Nielsen L, Hansen TM. Identifying unsaturated hydraulic parameters using an integrated data fusion approach on cross-borehole geophysical data. Vadose Zone J 2008;7:238-48.

[25] Looms MC, Jensen KH, Binley AM, Nielsen L. Monitoring unsaturated flow and transport using cross-borehole geophysical methods. Vadose Zone J 2008;7:227-37.

[26] Mertens J, Madsen H, Feyen L, Jacques D, Feyen J. Including prior information in the estimation of effective soil parameters in unsaturated zone modelling. J Hydrol 2004;294:251-69.

[27] Mertens J, Madsen H, Kristensen M, Jacques D, Feyen J. Sensitivity of soil parameters in unsaturated zone modelling and the relation between effective, laboratory and in situ estimates. Hydro Process 2005;19:1611-33.

[28] Metropolis N, Rosenbluth AW, Rosenbluth MN, Teller AH, Teller E. Equation of State Calculations by Fast Computing Machines. J Chem Phys 1953;21:1087-92.

[29] Mosegaard K, Tarantola A. Monte Carlo sampling of solutions to inverse problems. J Geophys Res 1995;100:12431-47.

[30] Mualem Y. A new model for predicting hydraulic conductivity of unsaturated porous-media. Water Resour Res 1976;12:513-22.

[31] Munoz-Carpena R, Regalado CM, Alvarez-Benedi J, Bartoli F. Field evaluation of the new Philip-Dunne permeameter for measuring saturated hydraulic conductivity. Soil Sci 2002;167:9-24.

[32] Pan LH, Wu LS. A hybrid global optimization method for inverse estimation of hydraulic parameters: Annealing-simplex method. Water Resour Res 1998;34:2261-9.

[33] Richards LA. Capillary conduction of liquids through porous mediums. J Appl Phys 1931;1:318-33.

[34] Ritter A, Hupet F, Munoz-Carpena R, Lambot S, Vanclooster M. Using inverse methods for estimating soil hydraulic properties from field data as an alternative to direct methods. Agr Water Manage 2003;59:77-96.

[35] Rucker DF, Ferre TPA. Parameter estimation for soil hydraulic properties using zero-offset borehole radar: Analytical method. Soil Sci Soc Am J 2004;68:1560-7.

[36] Sambridge M, Mosegaard K. Monte Carlo methods in geophysical inverse problems. Rev Geophys 2002;40:1009.

[37] Scharling M. DMI Technical report 99-12: Klimagrid Danmark, Nedbør, Lufttemperatur og potential fordampning 20*20 & 40*40 Km, metodebeskrivelse. 2010.

[38] Scharnagl B, Vrugt JA, Vereecken H, Herbst M. Bayesian inverse modelling of in situ soil water dynamics: using prior information about the soil hydraulic properties. Hydrol Earth Syst Sci Discuss 2011;8:2019-63.

[39] Scholer M, Irving J, Binley A, Holliger K. Estimating vadose zone hydraulic properties using ground penetrating radar: The impact of prior information. Water Resour Res 2011;47:W10512.

[40] Scholer M, Irving J, Looms MC, Nielsen L, Holliger K. Bayesian Markov Chain Monte Carlo inversion of time-lapse geophysical data to characterize the vadose zone at the Arrenaes field site, Denmark. Vadose Zone J 2012;in press.

[41] Schoups G, Vrugt JA. A formal likelihood function for parameter and predictive inference of hydrologic models with correlated, heteroscedastic, and non-Gaussian errors. Water Resour Res 2010;46:W10531.

[42] Schoups G, Vrugt JA, Fenicia F, de Giesen NCV. Corruption of accuracy and efficiency of Markov chain Monte Carlo simulation by inaccurate numerical implementation of conceptual hydrologic models. Water Resour Res 2010;46:W10530.

[43] Schultze B, Ippisch O, Huwe B, Durner W. Dynamic nonequilibrium during unsaturated water flow. In: Van Genuchten M, Leij FJ, Wu L, editors. Proc of the int workshop on characterization and measurement of the hydraulic properties of unsaturated porous media, Univ. of California, Riverside, CA; 1999.

[44] Simunek J, vanGenuchten MT. Estimating unsaturated soil hydraulic properties from multiple tension disc infiltrometer data. Soil Sci 1997;162:383-98.

[45] Simunek J, van Genuchten MT, Sejna M. Development and applications of the HYDRUS and STANMOD software packages and related codes. Vadose Zone J 2008;7:587-600.

[46] Sisson JB, Vangenuchten MT. An Improved Analysis of Gravity Drainage Experiments for Estimating the Unsaturated Soil Hydraulic Functions. Water Resour Res 1991;27:569-75.

[47] Steenpass C, Vanderborght J, Herbst M, Simunek J, Vereecken H. Estimating Soil Hydraulic Properties from Infrared Measurements of Soil Surface Temperatures and TDR Data. Vadose Zone J 2010;9:910-24.

[48] Topp GC, Davis JL, Annan AP. Electromagnetic determination of soil-water content-measurement in coaxial transmission-lines. Water Resour Res 1980;16:574-82.

[49] Tseng PH, Jury WA. Simulation of Field Measurement of Hydraulic Conductivity in Unsaturated Heterogeneous Soil. Water Resour Res 1993;29:2087-99.

[50] van Genuchten M. A Closed-form Equation for Predicting the Hydraulic Conductivity of Unsaturated Soils. Soil Sci Soc Am J 1980;44:892-8.

[51] Van Genuchten MT, Leij FJ. Indirect methods for estimating the hydraulic properties of unsaturated soils. Proceedings of the International Workshop on Indirect Methods for Estimating the Hydraulic Properties of Unsaturated Soils, Riverside California, 1989.

[52] Vrugt JA, Bouten W, Weerts AH. Information content of data for identifying soil hydraulic parameters from outflow experiments. Soil Sci Soc Am J 2001;65:19-27.

[53] Vrugt JA, Stauffer PH, Wohling T, Robinson BA, Vesselinov VV. Inverse modeling of subsurface flow and transport properties: A review with new developments. Vadose Zone J 2008;7:843-64.

[54] Wildenschild D, Jensen KH, Hollenbeck KJ, Illangasekare TH, Znidarcic D, Sonnenborg T, et al. A two-stage procedure for determining unsaturated hydraulic characteristics using a syringe pump and outflow observations. Soil Sci Soc Am J 1997;61:347-59.

[55] Wildenschild D, Hopmans JW, Simunek J. Flow rate dependence of soil hydraulic characteristics. Soil Sci Soc Am J 2001;65:35-48.

[56] Winship P, Binley AM, Gomez D. Flow and transport in the unsaturated Sherwood Sandstone: characterization using cross-borehole geophysical methods. 2006;263:219-31.

[57] Wohling T, Vrugt JA. Combining multiobjective optimization and Bayesian model averaging to calibrate forecast ensembles of soil hydraulic models. Water Resour Res 2008;44:W12432.

[58] Wöhling T, Vrugt JA. Multiresponse multilayer vadose zone model calibration using Markov chain Monte Carlo simulation and field water retention data. Water Resour Res 2011;47:W04510.

Figure Captions

Figure 1: Net daily infiltration estimates at the Arrenaes site over the considered natural loading period from 01/07/2004 to 30/07/2005. Data obtained from the Danish Meterological Institute [37].

Figure 2: Synthetic time-lapse ZOP crosshole GPR traveltime data corresponding to the layered environment described in Table 1 for the three infiltration cases described in Table 2.

Figure 3: Shannon entropy measure calculated for the VGM parameters in each subsurface layer from the different sets of posterior samples obtained in our synthetic study. The red, green, and blue curves represent the NL, F1, and F2 infiltration cases, respectively. Results are plotted as a function of the time-lapse scenarios described in Table 3. Scenario 0 corresponds to $H_{max} = \log_2(120) = 6.9$, and represents the uniform prior distribution considered for each parameter.

Figure 4: Mean and standard deviation calculated for the VGM parameters in Layer 3 from the different sets of posterior samples obtained in our synthetic study. The red, green, and blue colors represent the NL, F1, and F2 infiltration cases, respectively. Results are plotted as a function of the time-lapse scenarios described in Table 3. The true parameter values are shown by the thin black lines.

Figure 5: 95% uncertainty bounds for the water retention function in Layer 3 predicted by the prior (grey) and posterior (green) sets of VGM parameter samples for each considered infiltration and time period scenario. The curves corresponding to the "true" parameters are shown in black.

Figure 6: 95% uncertainty bounds for the hydraulic conductivity function in Layer 3 predicted by the prior (grey) and posterior (green) sets of VGM parameter samples for each considered infiltration and time period scenario. The curves corresponding to the "true" parameters are shown in black.

Figure 7: (a) Location of the Arrenaes field site and (b) installed borehole configuration at the site. Modified from Looms et al. [25].

Figure 8: (a) Grain size statistics and (b) granulometric composition obtained from core analysis of borehole A at the Arrenaes site [15].

Figure 9: Time-lapse ZOP crosshole GPR traveltime data measured at the Arreneas field site for the three infiltration scenarios.

Figure 10: Shannon entropy measure calculated for the VGM parameters in each subsurface layer from the different sets of posterior samples obtained in our field study. The red, green, and blue curves represent the NL, F1, and F2 infiltration cases, respectively. Results are plotted as a function of the time-lapse scenarios described in Table 7. Scenario 0 corresponds to H_{max}=log2(200)=7.64, and represents the uniform prior distribution considered for each parameter.

Figure 11: Mean and standard deviation calculated for the VGM parameters in Layer 3 from the different sets of posterior samples obtained in our field study. The red, green, and blue colors represent the NL, F1, and F2 infiltration cases, respectively. Results are plotted as a function of the time-lapse scenarios described in Table 7.

Figure 12: 95% uncertainty bounds for the water retention function in Layer 3 predicted by the prior (grey) and posterior (green) sets of VGM parameter samples for each considered infiltration and time period scenario.

Figure 13: 95% uncertainty bounds for the hydraulic conductivity function in Layer 3 predicted by the prior (grey) and posterior (green) sets of VGM parameter samples for each considered infiltration and time period scenario.

Table captions

Table 1: Subsurface layer configuration and corresponding "true" VGM parameter values considered in our synthetic study.

Table 2: Details concerning the three different infiltration cases considered in our synthetic study.

Table 3: Different time periods considered for the inversion of the synthetic GPR traveltime data corresponding to the three infiltration cases in Table 2. For each scenario all of the data considered in the previous scenarios were included (i.e., Scenario 1 for the NL case considered the GPR profile collected at 1 month, whereas Scenario 3 considered the GPR profiles collected at 1, 3 and 6 months).

Table 4: Lower and upper bounds of the prior uniform distributions assumed for the VGM parameters in each layer for all inversions performed in this study.

Table 5: Geological structure defined for the Arrenaes field site based on the grain size analysis shown in Figure 8 [15].

Table 6: Details concerning the three different infiltration experiments conducted at the Arrenaes field site. Note that infiltration was continuous throughout the data measurement period.

Table 7: Different time periods considered for the inversion of the field GPR traveltime data collected at the Arrenaes site corresponding to the three infiltration cases in Table 6. For each scenario all of the data considered in the previous scenarios were included.
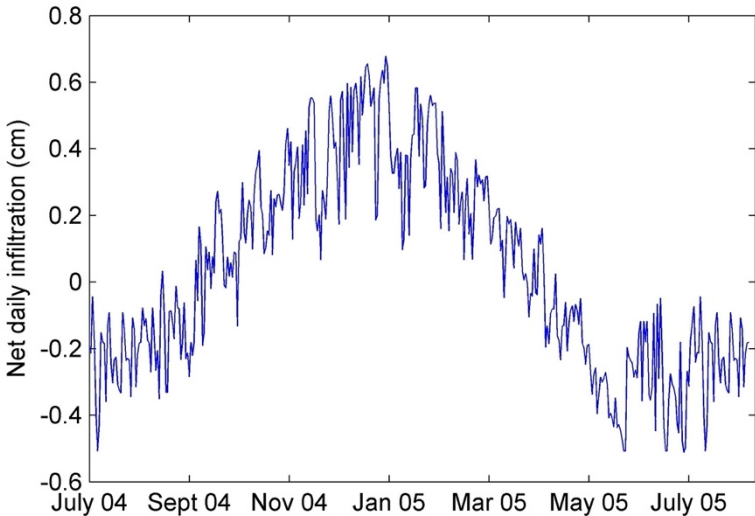
FIGURES

Figure 1: Net daily infiltration estimates at the Arrenaes site over the considered natural loading period from 01/07/2004 to 30/07/2005. Data obtained from the Danish Meterological Institute [3].
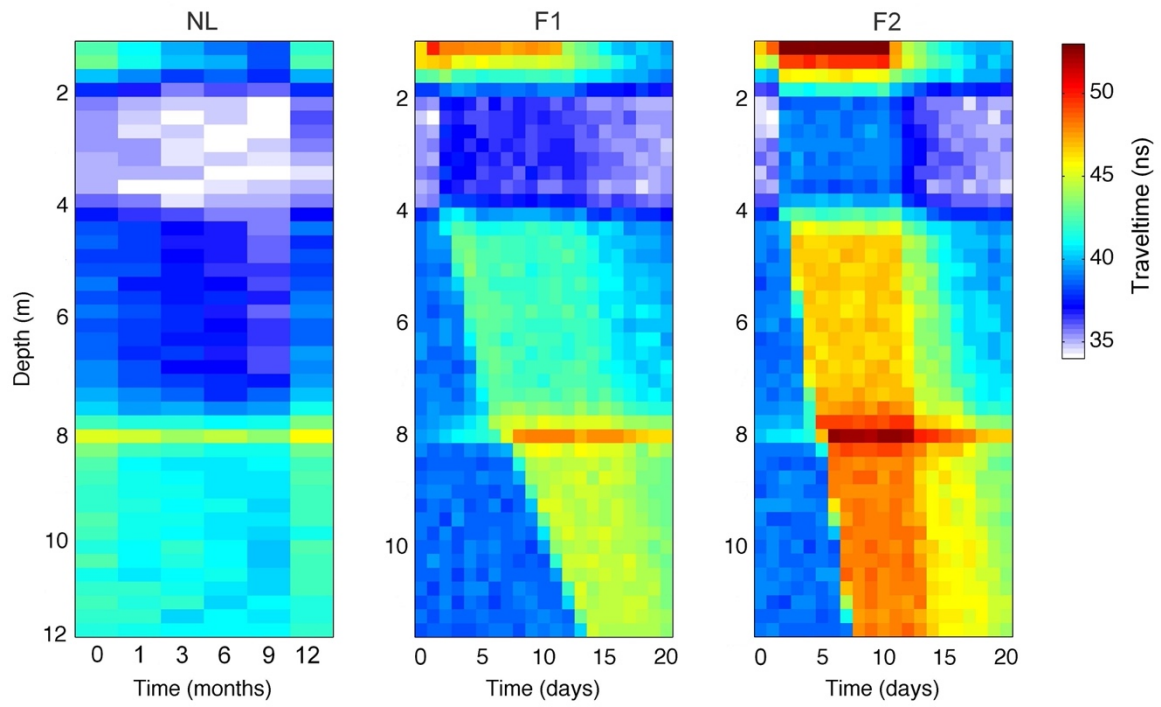
Figure 2: Synthetic time-lapse ZOP crosshole GPR traveltime data corresponding to the layered environment described in Table 1 for the three infiltration cases described in Table 2.
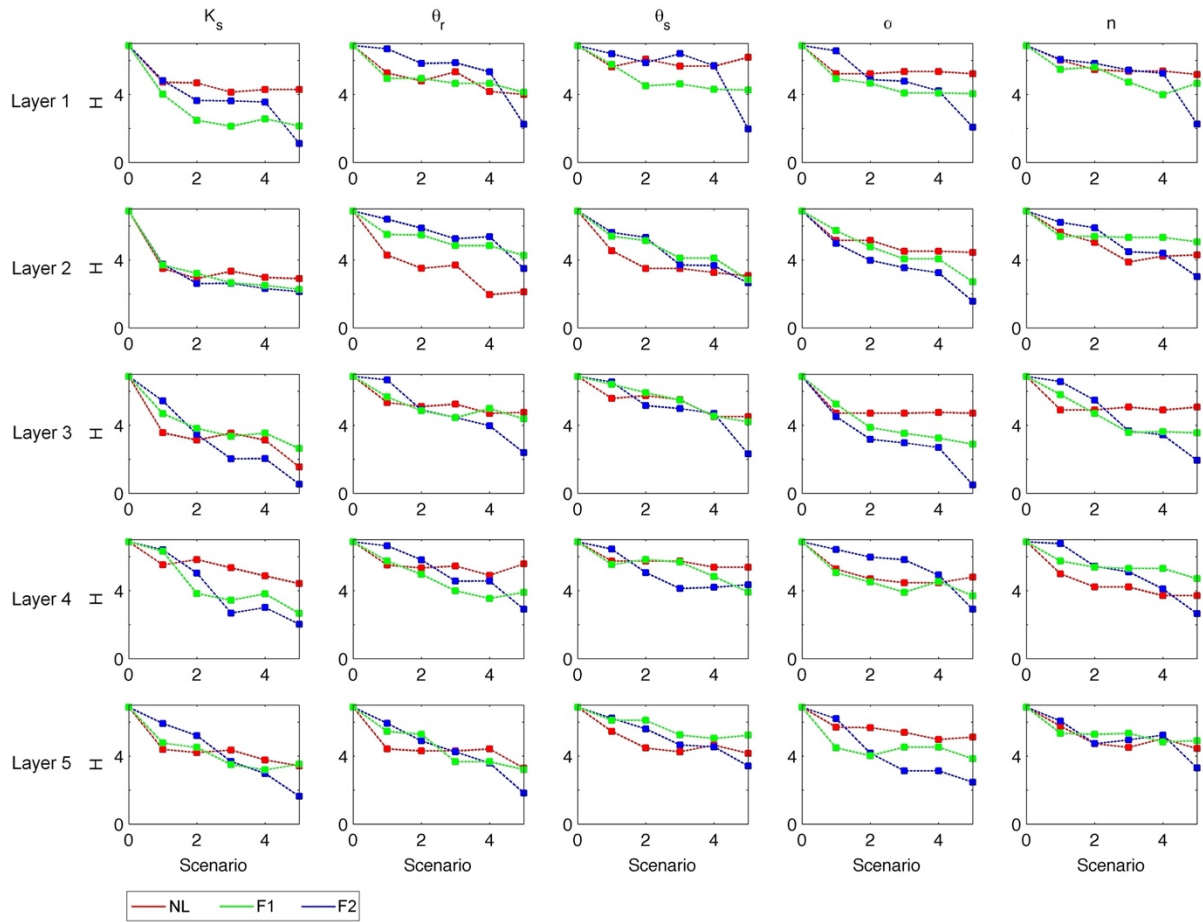
Figure 3: Shannon entropy measure calculated for the VGM parameters in each subsurface layer from the different sets of posterior samples obtained in our synthetic study. The red, green, and blue curves represent the NL, F1, and F2 infiltration cases, respectively. Results are plotted as a function of the time-lapse scenarios described in Table 3. Scenario 0 corresponds to $H_{max} = \log_2(120) = 6.9$, and represents the uniform prior distribution considered for each parameter.

Figure 4: Mean and standard deviation calculated for the VGM parameters in Layer 3 from the different sets of posterior samples obtained in our synthetic study. The red, green, and blue colors represent the NL, F1, and F2 infiltration cases, respectively. Results are plotted as a function of the time-lapse scenarios described in Table 3. The true parameter values are shown by the thin black lines. The extent of the vertical axis represents the range of the prior distributions in Table 4.
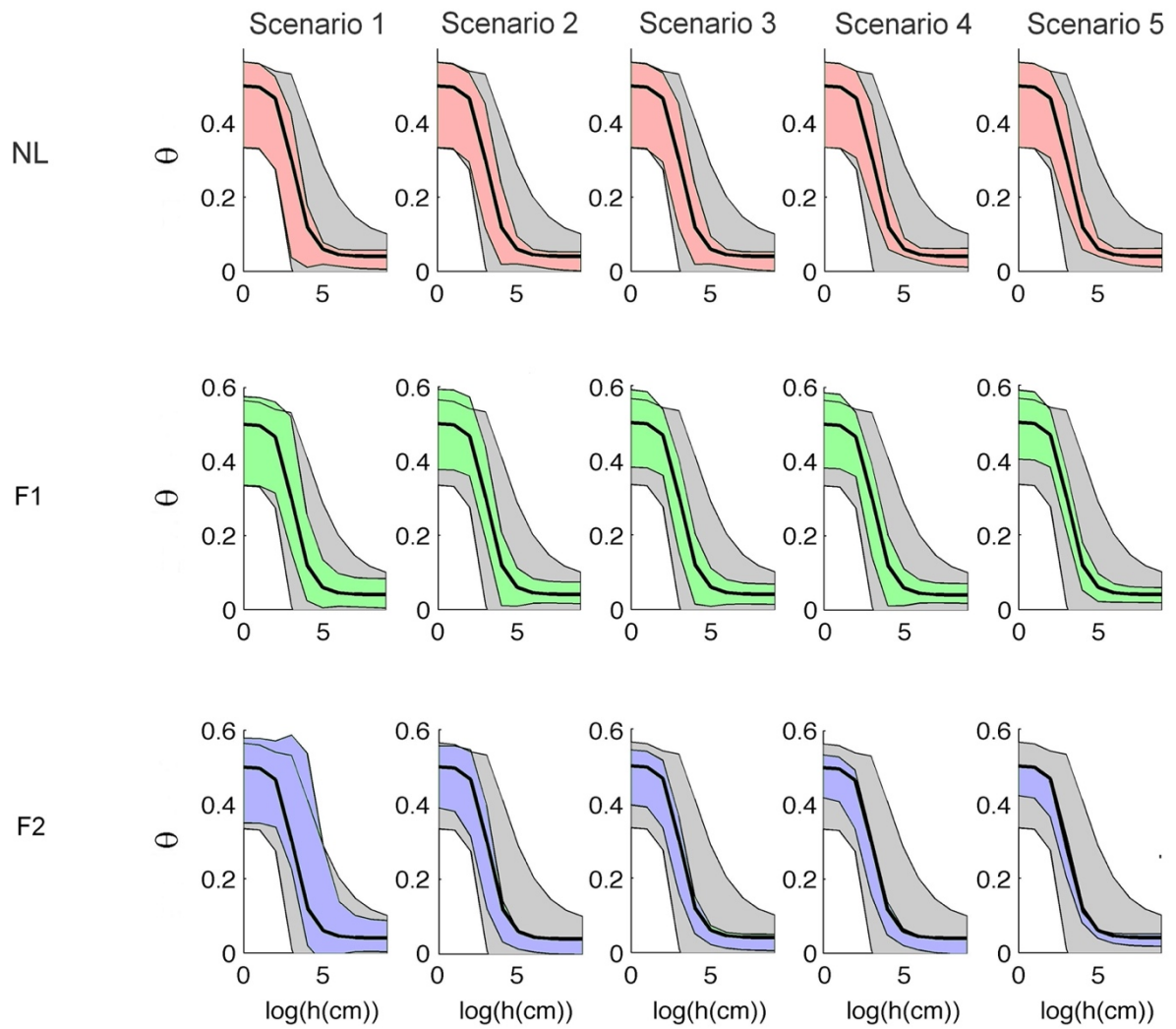
Figure 5: 95% uncertainty bounds for the water retention function in Layer 3 predicted by the prior (grey) and posterior (green) sets of VGM parameter samples for each considered infiltration and time period scenario. The curves corresponding to the "true" parameters are shown in black.
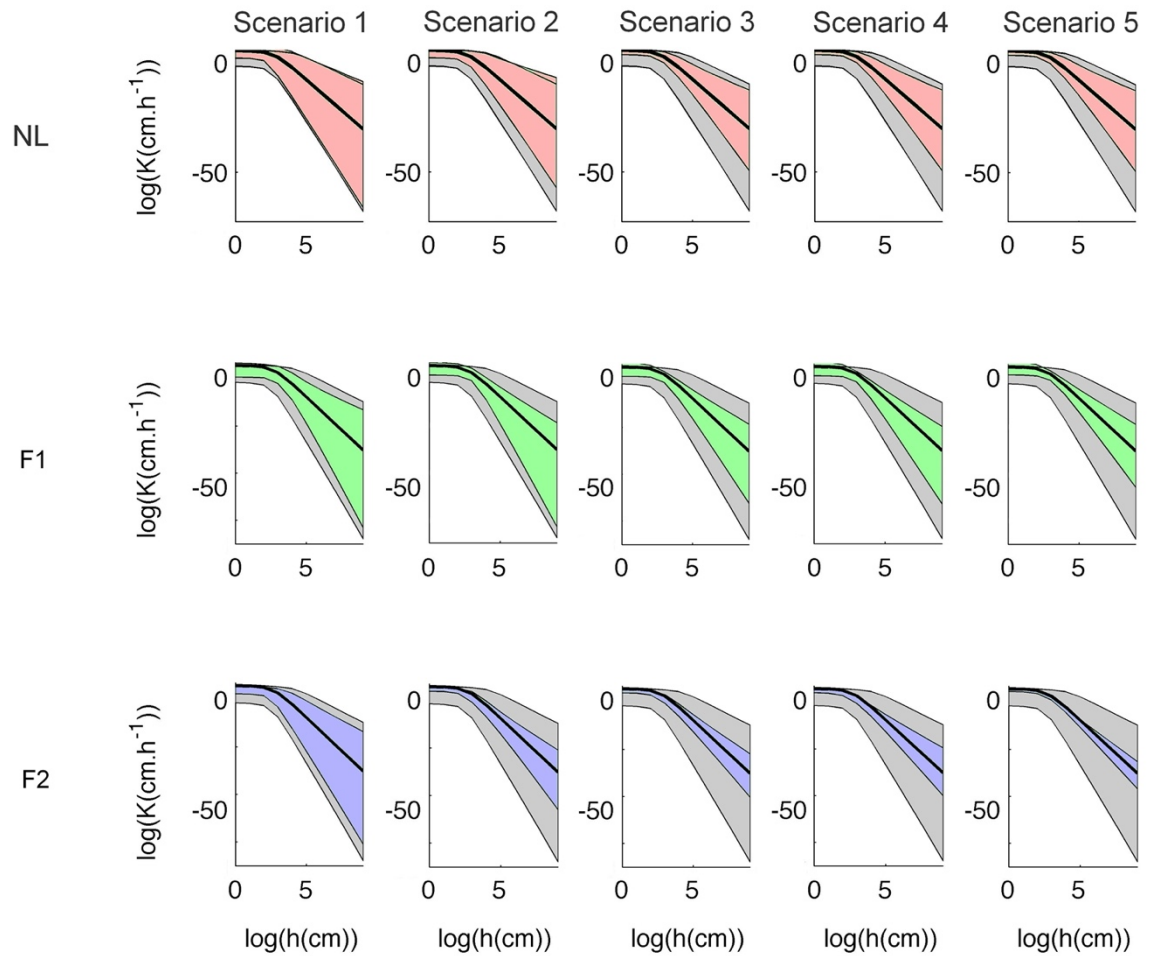
Figure 6: 95% uncertainty bounds for the hydraulic conductivity function in Layer 3 predicted by the prior (grey) and posterior (green) sets of VGM parameter samples for each considered infiltration and time period scenario. The curves corresponding to the "true" parameters are shown in black.
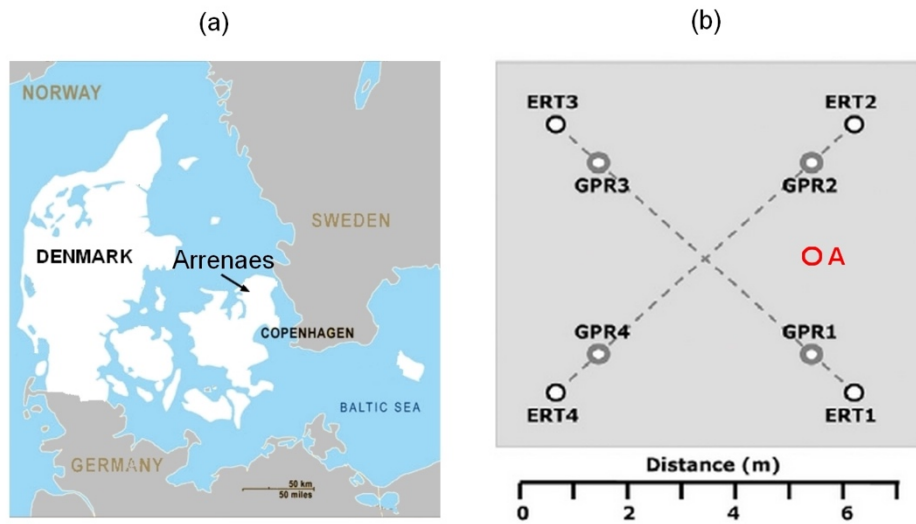
Figure 7: (a) Location of the Arrenaes field site and (b) installed borehole configuration at the site. Modified from Looms et al. [2].
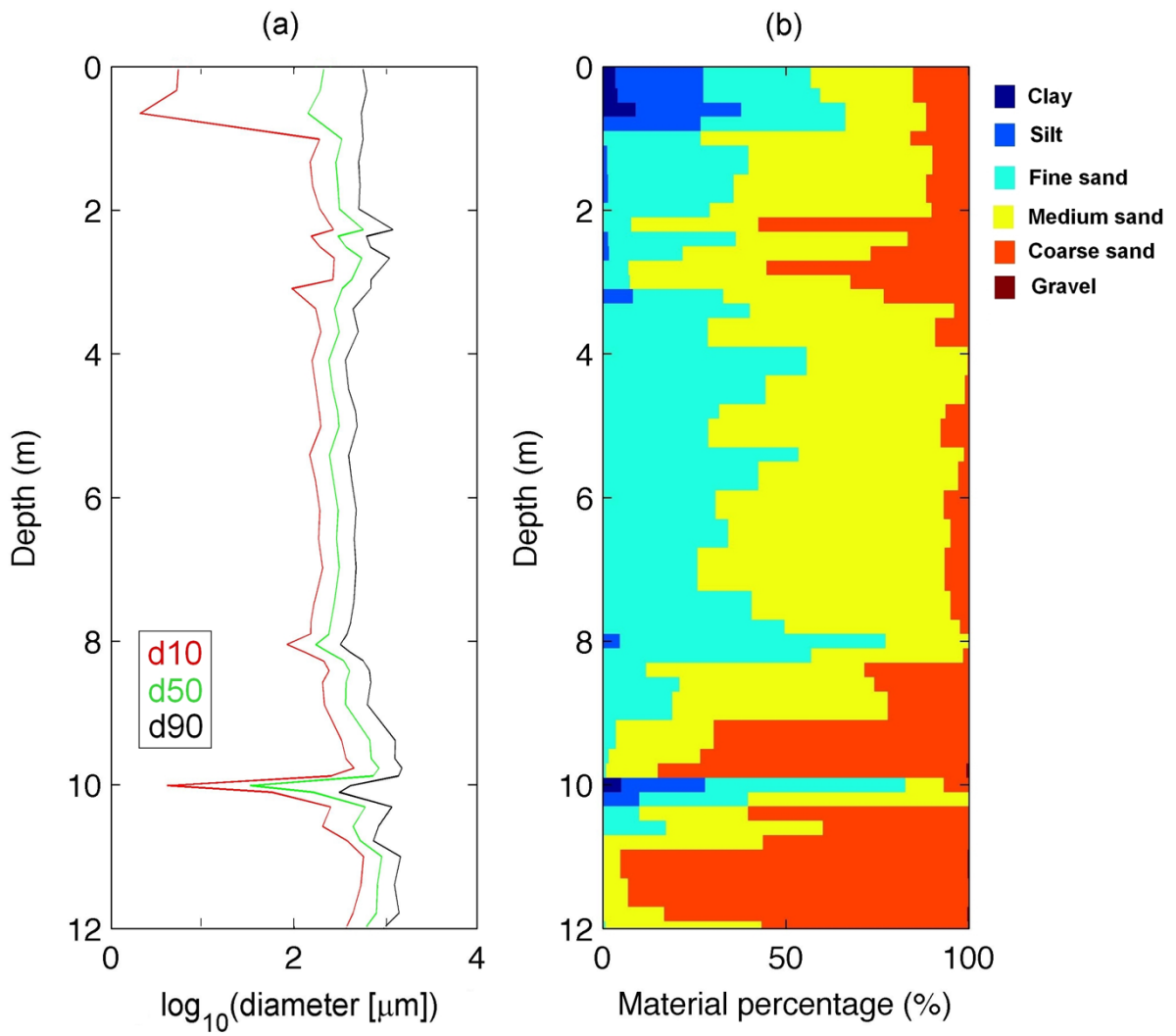
Figure 8: (a) Grain size statistics and (b) granulometric composition obtained from core analysis of borehole A at the Arrenaes site [1].
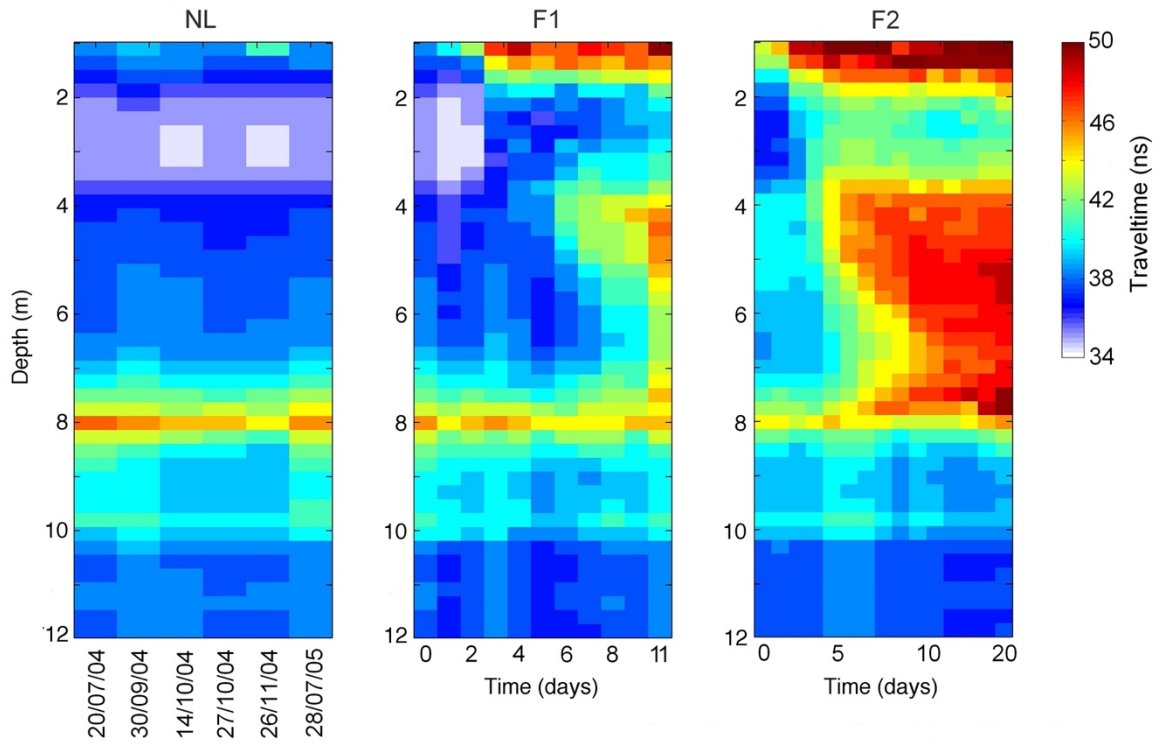
Figure 9: Time-lapse ZOP crosshole GPR traveltime data measured at the Arreneas field site for the three infiltration scenarios.
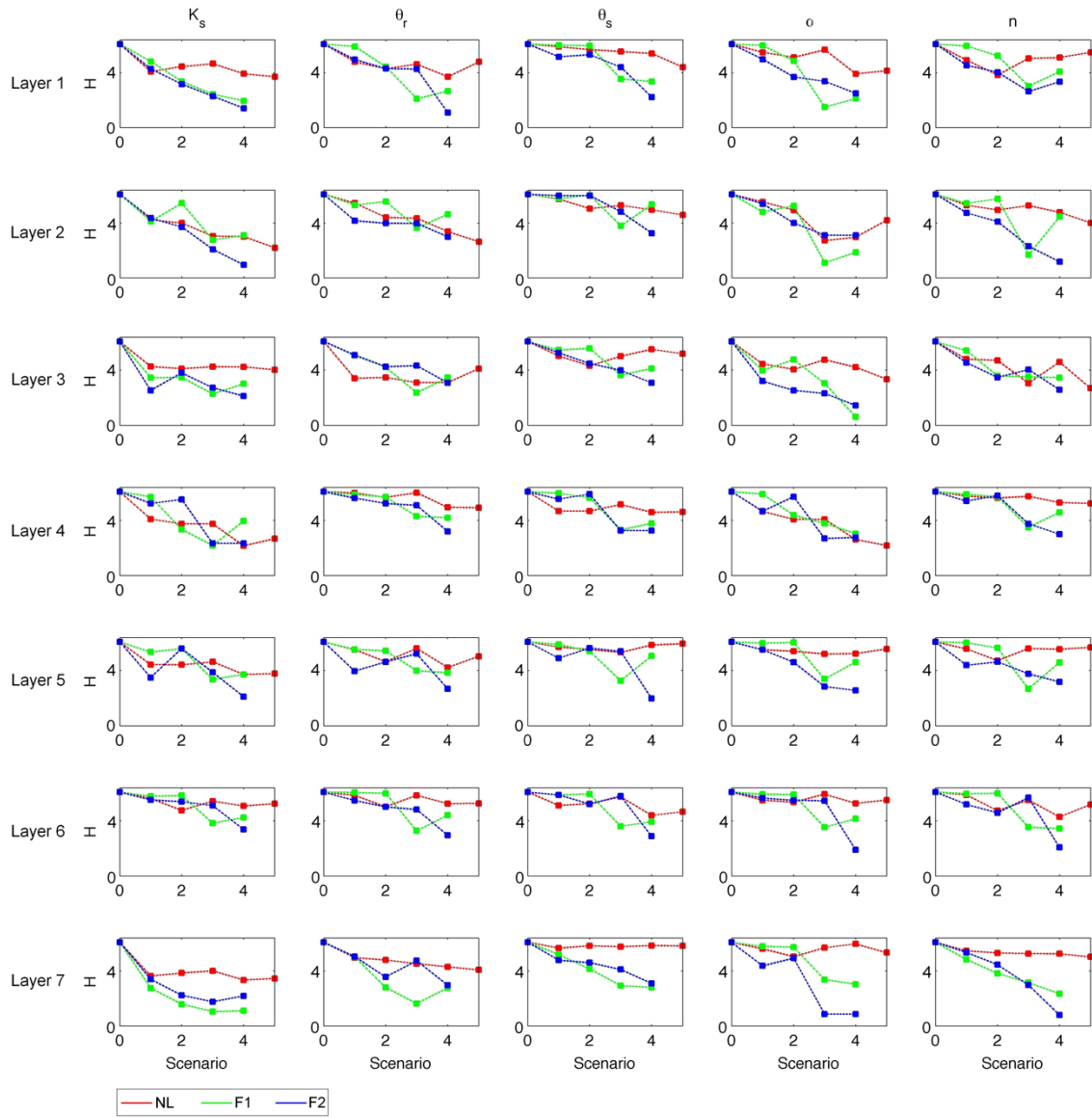
Figure 10: Shannon entropy measure calculated for the VGM parameters in each subsurface layer from the different sets of posterior samples obtained in our field study. The red, green, and blue curves represent the NL, F1, and F2 infiltration cases, respectively. Results are plotted as a function of the time-lapse scenarios described in Table 7. Scenario 0 corresponds to H_{max}=log2(200)=7.64, and represents the uniform prior distribution considered for each parameter.

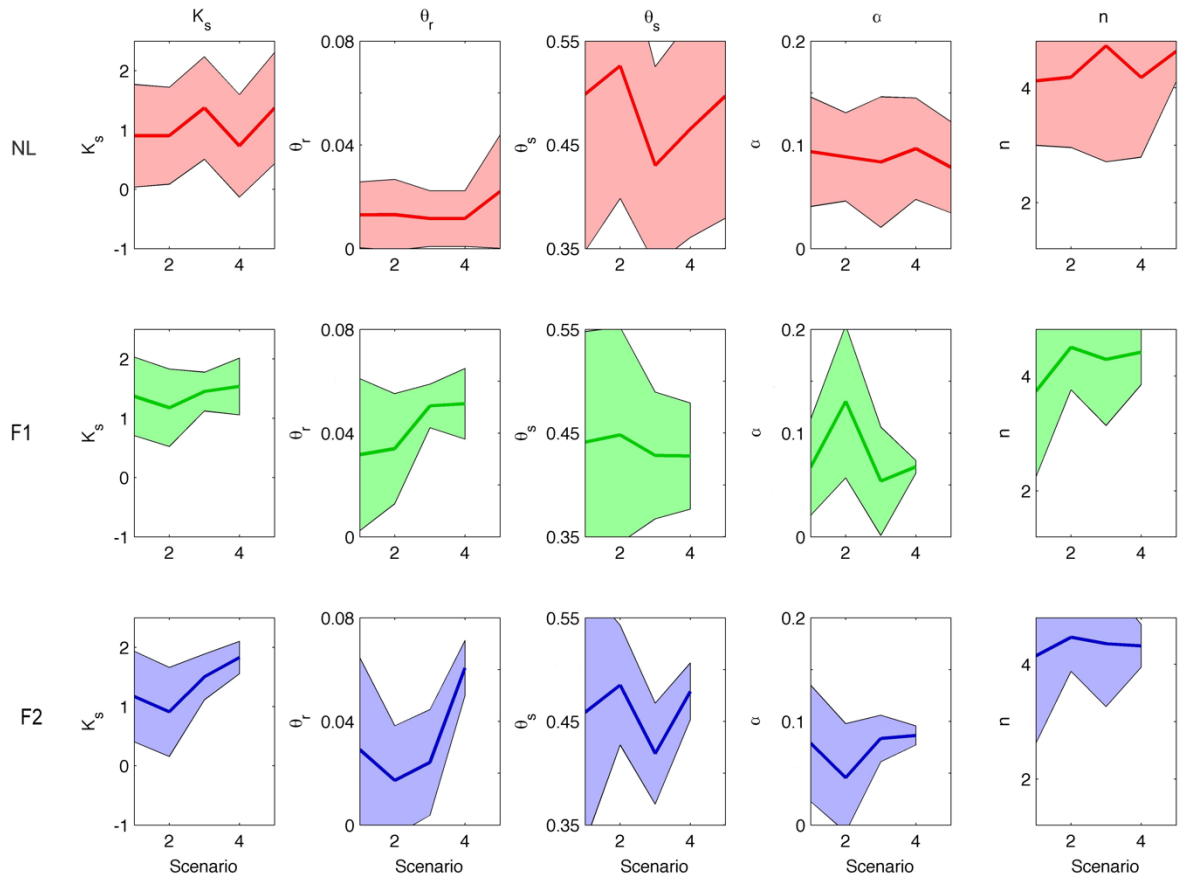Figure 11: Mean and standard deviation calculated for the VGM parameters in Layer 3 from the different sets of posterior samples obtained in our field study. The red, green, and blue colors represent the NL, F1, and F2 infiltration cases, respectively. Results are plotted as a function of the time-lapse scenarios described in Table 7. The extent of the vertical axis represents the range of the prior distributions in Table 4.

Figure 12: 95% uncertainty bounds for the water retention function in Layer 3 predicted by the prior (grey) and posterior (green) sets of VGM parameter samples for each considered infiltration and time period scenario.
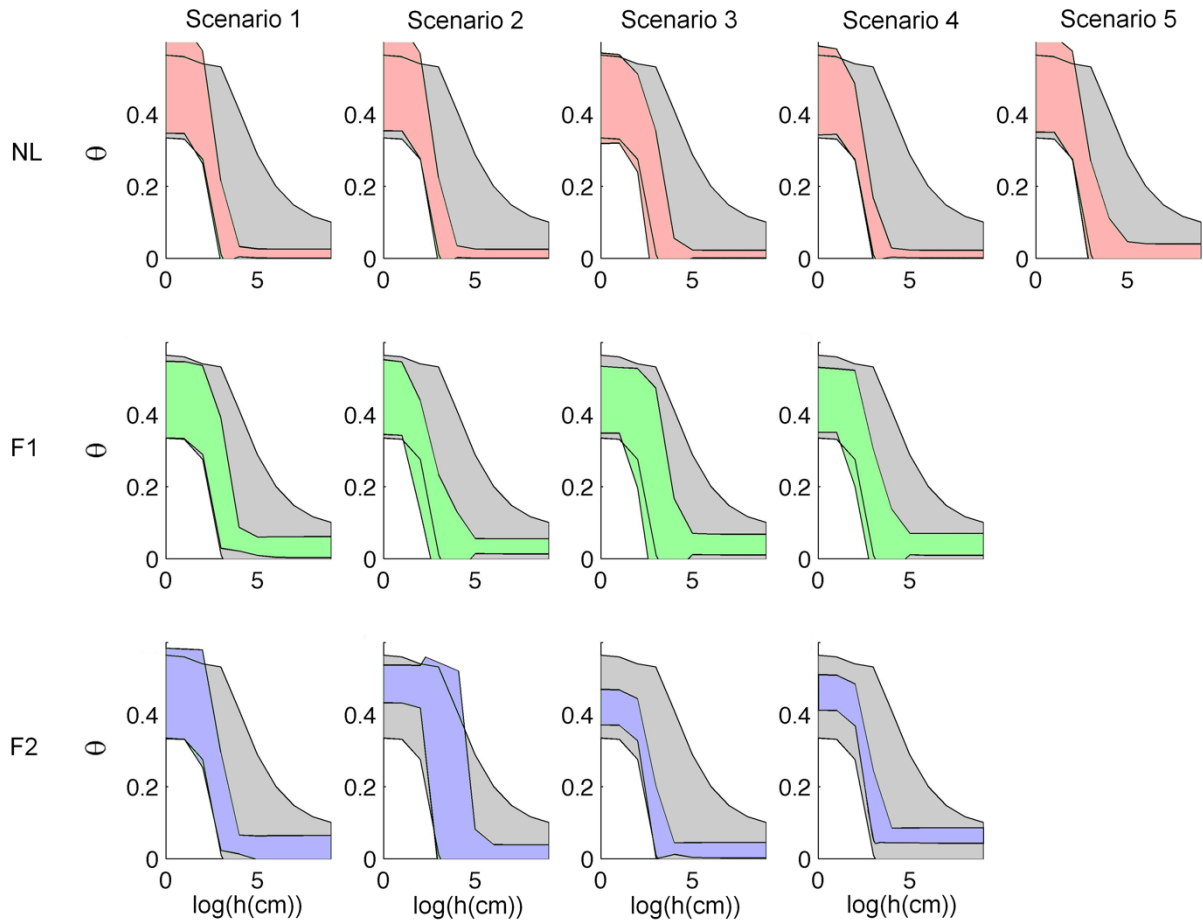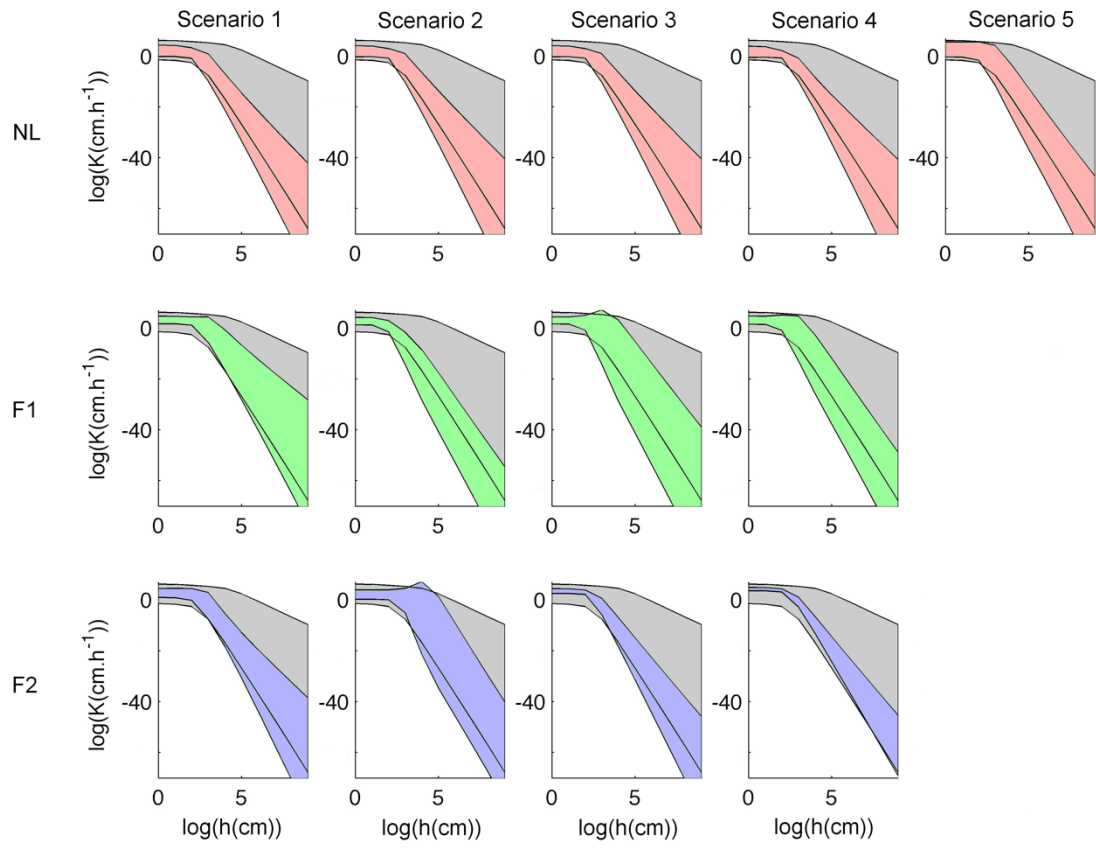
Figure 13: 95% uncertainty bounds for the hydraulic conductivity function in Layer 3 predicted by the prior (grey) and posterior (green) sets of VGM parameter samples for each considered infiltration and time period scenario.

TABLES

Table 1: Subsurface layer configuration and corresponding "true" VGM parameter values considered in our synthetic study.

Layer	Depth (m)	Log10(K_s (cm·h⁻¹))	θ_r	θ_s	α (cm⁻¹)	n
1	0-2	1.5	0.06	0.53	0.15	3.5
2	2-3.66	2.3	0.05	0.37	0.05	4.3
3	3.66-7.75	2.2	0.04	0.52	0.06	2.4
4	7.75-8.25	2.2	0.10	0.49	0.15	2.7
5	8.25-12	2.5	0.07	0.51	0.18	3.6

Table 2: Details concerning the three different infiltration cases considered in our synthetic study.

Case	Total simulation time	Length of infiltration period	Net infiltration rate	GPR data collection times
NL	12 months	12 months	See Figure 1	1, 3, 6, 9, 12 months
F1	20 days	10 days	0.1 cm/h	Daily
F2	20 days	10 days	0.4 cm/h	Daily

Table 3: Different time periods considered for the inversion of the synthetic GPR traveltime data corresponding to the three infiltration cases in Table 2. For each scenario all of the data considered in the previous scenarios were included (i.e., Scenario 1 for the NL case considered the GPR profile collected at 1 month, whereas Scenario 3 considered the GPR profiles collected at 1, 3 and 6 months).

	NL	# of GPR profiles	F1	# of GPR profiles	F2	# of GPR profiles	
Scenario 1	1 month	1	1 day	1	1 day	1	Infiltration
Scenario 2	3 months	2	4 days	2	4 days	2	
Scenario 3	6 months	3	7 days	3	7 days	3	
Scenario 4	9 months	4	10 days	4	10 days	4	
Scenario 5	12 months	5	15 days	5	15 days	5	Drainage

Table 4: Lower and upper bounds of the prior uniform distributions assumed for the VGM parameters in each layer for all inversions performed in this study.

VGM parameter	Lower bound	Upper bound
Log10(K$_s$ (cm·h^{-1}))	-1	2.5
θ$_r$	0	See text
θ$_s$	0.35	0.55
α (cm^{-1})	0	0.2
n	1.1	4.8

Table 5: Geological structure defined for the Arrenaes field site based on the grain size analysis shown in Figure 8 [1].

Layer	Depth (m)	Main material
1	0-2	Medium to fine sand
2	2-3.66	Medium to coarse sand
3	3.66-7.75	Medium to fine sand
4	7.75-8.25	Fine to medium sand
5	8.25-10	Medium to coarse sand
6	10-10.16	Fine sand to silt
7	10.16-12	Coarse sand

Table 6: Details concerning the three different infiltration experiments conducted at the Arrenaes field site. Note that infiltration was continuous throughout the data measurement period.

Case	Total experiment time	Net infiltration rate	Starting date	GPR data collection times
NL	12 months	See Figure 1	20/07/04	20/07/04, 30/09/04, 14/10/04, 27/10/04, 26/11/04, 28/07/05
F1	11 days	0.20 cm/h	31/07/05	Daily until Day 9, and then on Day 11
F2	20 days	0.36 cm/h	18/10/05	Daily until Day 10, and then on Days 13, 15, 17 and 20

Table 7: Different time periods considered for the inversion of the field GPR traveltime data collected at the Arrenaes site corresponding to the three infiltration cases in Table 6. For each scenario all of the data considered in the previous scenarios were included.

	NL	# of GPR profiles	F1	# of GPR profiles	F2	# of GPR profiles
Starting date	20/07/04	-	31/07/05	-	18/10/05	-
Scenario 1	30/09/04	1	01/08/05	1	19/10/05	1
Scenario 2	14/10/04	2	04/08/05	2	22/10/05	2
Scenario 3	27/10/04	3	07/08/05	3	25/10/05	3
Scenario 4	26/11/04	4	11/08/05	4	28/10/05	4
Scenario 5	28/07/05	5	-	-	-	-